APPLICATION OF CONFORMAL MAPPING TO SCATTERING AND DIFFRACTION PROBLEMS

by
Soonsung Hong

A dissertation submitted in partial fulfillment
of the requirements for the degree of
Doctor of Philosophy in the
University of Michigan
1965

Doctoral Committee:

Professor Chiao-Min Chu, Chairman
Professor Charles L. Dolph
Doctor Raymond F. Goodrich
Associate Professor Andrejs Olte
Doctor Thomas B. A. Senior
Professor C. Bruce Sharpe

RL-259 = RL-259

ABSTRACT

APPLICATION OF CONFORMAL MAPPING TO SCATTERING AND DIFFRACTION PROBLEMS

BY

SOONSUNG HONG

The problem of finding the scattered and diffracted fields of a plane wave normally incident on an infinite cylinder with arbitrary cross section presents considerable difficulty. The mathematical problem involves finding a solution of the scalar wave equation which satisfies both the boundary condition at the surface of the cylinder and the radiation condition at infinity.

This thesis describes a boundary perturbation method, based on conformal mapping, which can be used to obtain an approximate solution. Firstly, the domain external to the scattering body is conformally mapped into another domain external to a geometrically simpler cylinder for which the Green's function satisfying the prescribed boundary condition is known. Such a conformal transformation preserves the right angle between the direction of propagation of a wave and its wavefront. Furthermore, the characteristics of the geometry of the boundary are reflected in the behavior of the mapping function there. Secondly, a Fredholm integral equation of the second kind governing the scattered field is formulated. The solution of this equation can be obtained by the method of successive approximation, provided that both original and transformed boundaries have continuous tangents and that the distance between the two curves is sufficiently small in

comparison with the wavelength. This integral equation method proves to be particularly effective in dealing with fields diffracted by discontinuities both in curvature and in derivatives of the curvature, and in showing the effects of smooth, shallow corrugations of the scattering body. Various expressions for the fields diffracted by the discontinuity in curvature are obtained by varying both the observation point and the position of the discontinuity in curvature in reference to the direction of incidence.

The attention in this thesis is primarily confined to the case of Dirichlet boundary condition. The extension of the conformal mapping method to the case of Neumann boundary condition is also briefly discussed.

ACKNOWLEDGEMENTS

The candidate wishes to express his appreciation for the assistance and guidance given him by Professor C. M. Chu, chairman of the doctoral committee.

The author is especially indebted to Dr. R. F. Goodrich who brought this problem to his attention and provided valuable guidance.

Thanks are also due to Professors C. L. Dolph, A. Olte and C. B. Sharpe, and to Dr. T. B. A. Senior for helpful discussions and correcting the manuscript.

The research reported in this thesis was supported by the National Aeronautics and Space Administration under Grant NsG-444 with the NASA-Langley Research Center.

Finally, the author would like to acknowledge the assistance and encouragement received from the entire staff of the Radiation Laboratory at the University of Michigan, particularly from Mrs. Louis Harrell and Mrs. Marvin Griffin who typed the manuscript.

TABLE OF CONTENTS

LIST OF TABLES

LIST OF ILLUSTRATIONS

CHAPTER I

INTRODUCTION

In this thesis, the scattering and diffraction problem of a plane electromagnetic wave normally incident on a perfectly conducting infinite cylinder in a homogeneous isotropic medium and polarized parallel to the cylinder axis is investigated. The boundary of the cylinder is assumed to have a continuous tangent everywhere. The mathematical problem involves finding a solution of the scalar wave equation which satisfies both the boundary condition and the radiation condition at infinity.

Exact solutions are available, through the method of separation of variables, for only a few simple shapes such as the circular, the elliptic or the parabolic cylinder. The objective of this thesis is to study an approximation method of obtaining far field expressions of scattered and diffracted waves for more general shapes of the cylinder cross-section by means of conformal mapping.

In the past, various approximation methods have been developed for low and high frequency scattering. In the case of low frequency scattering, the characteristic dimension of the body is assumed to be much smaller than the wavelength. Van Bladel[1] introduced a quasi-static method that gives only the initial term of an expansion in a series of powers of $\log k$ and k (k = wave number). This term is not dependent on the geometrical shape of the cylinder, but only on its size.

A considerable effort has been devoted to the solution of the problem of high frequency scattering. (MacDonald[2], Fock[3],[4], Franz and Deppermann[5], Franz[6], Keller[7], Ursell[8], Goriainov[9], Goodrich[10], Weinstein and Fedorov[11],

and Felsen[12]). In the case of high frequency approximations, the characteristic dimension of the scattering body is assumed large in comparison with the wavelength.

When a high-frequency wave is incident on a perfectly conducting body, a first approximation is found using the method of physical optics. In this method one assumes that the current on the surface at a point in the illuminated region is the same as would be induced on an infinite plane occupying the position of the tangent plane, and is identically zero in the shadow region. It is well known that this approximation yields a very poor picture of the behavior of the field in the shadow region and near the shadow boundary.

An improved approximation method for the behavior of the field near the shadow boundary is that of Fock. He assumes that the boundary and the wave equation near the shadow boundary can be approximated by a parabola and a parabolic equation, respectively. This method gives a smooth transition from the geometrical optics term to an exponentially decaying field, the so-called creeping wave, as the observation point moves across the shadow boundary. Fock's method requires continuity of curvature of the boundary.

Another improved method of approximation for high frequency has been developed by Keller and his colleagues in their geometrical theory of diffraction. The theory postulates that, in addition to the incident and reflected rays of geometrical optics, there exist diffracted rays. These rays are produced when an incident ray hits a kink or vertex on the scattering surface, or when it impinges tangentially on a smoothly curved boundary. Their excitation amplitude depends on the incident field as well as on properties of the surface

in the immediate neighborhood of the point of diffraction. Consequently, the diffraction coefficient (the ratio between the diffracted field and the incident field near the point of diffraction) may be determined from the rigorous solution of canonical problems. The latter are simplified problems in which occur only the local properties of the field and of the scattering surface.

Diffraction coefficients of both the shadow boundary of the curved surface with continuous curvature, and the wedge are known (Oberhettinger[13] and Keller[14]); but few people have studied diffraction problems of waves by an edge* with discontinuity in derivatives of the tangent, that is, discontinuity in curvature or in its derivatives.

Weston[15],[16] obtained the effect of a discontinuity in curvature in high frequency scattering. He studied the case in which the point of discontinuity in curvature is in the illuminated region and the total field on the boundary satisfies the Neumann boundary condition.

In the above brief review of past work, none of the approximation methods attempt to obtain desired solutions by mapping the given geometry of the scatterer surface into a geometrically simpler one.

In the past, conformal mapping has been extensively used to simplify the geometrical shape of the given boundary, in order to solve boundary value problems for both Laplace's equation and the waveguide problem (the reader

---

* The term 'edge' is used in a general sense. Any point where the boundary has a discontinuity in the curvature or in its derivatives is called an edge.

is referred to papers by Rice[17],[18], Weinstein[19], Mittra[20] and Meinke[21]. The approximation method which has been applied in the theory of waveguides is essentially concerned with quasi-static techniques, that is, low frequency approximation techniques.

Recently Jones[22] showed that the asymptotic solution of the wave equation, which is obtained by the W. K. B. J. L. method for high frequency scattering, is invariant under conformal mapping, provided that the mapping function is conformal everywhere including at the boundary (see Section 2. 2).

Garabedian[23] gave one of the first convincing proofs of the usefulness of the application of conformal mapping to scattering and diffraction by a body having singularities. The success of the method which he developed depends on the fact that the derivation of a Fredholm integral equation governing the scattered field does not require the mapping function to be conformal on the boundary.

Furthermore, the characteristics of the geometry of the boundary are reflected in the behavior of the mapping function there. Mathematically, the order of singularity of the mapping function on the boundary is determined by the property of the geometry of the boundary itself (see Warschawski's work[24] and Section 5. 2 of this thesis for further details). This property enables us to study the effect of geometrical irregularities of the boundary on diffracted fields.

In this thesis, as specific examples, Garabedian's integral equation is applied to study effects of certain irregularities of the boundary, such as discontinuities in curvature or high order derivatives, or smooth, shallow corrugations, on the scattering and diffraction of waves.

We shall confine our attention entirely to the case of Dirichlet boundary condition. The extension of the conformal mapping method to the case of Neumann boundary condition is discussed in Chapter 6.

CHAPTER II

REPRESENTATION OF SCATTERED FIELDS

In this chapter, a boundary value problem of the wave equation for a scattered field is formulated. After applying conformal mapping, Garabedian's integral equation is derived and the method of solving the integral equation is discussed. Both the derivation of Garabedian's integral equation and the definition of the norm of the kernel are a little different from the derivation and definition given in Garabedian's original paper[23].

The rationalized M.K.S. system of the units is used and the time dependence factor $e^{-i\omega t}$ is omitted.

2.1 Formulation of the Problem

Let the plane wave $\underline{E}_{in} = \hat{z}\, e^{ik\xi}$ be incident on a perfectly conducting cylinder with an arbitrary shape of the cross-section.

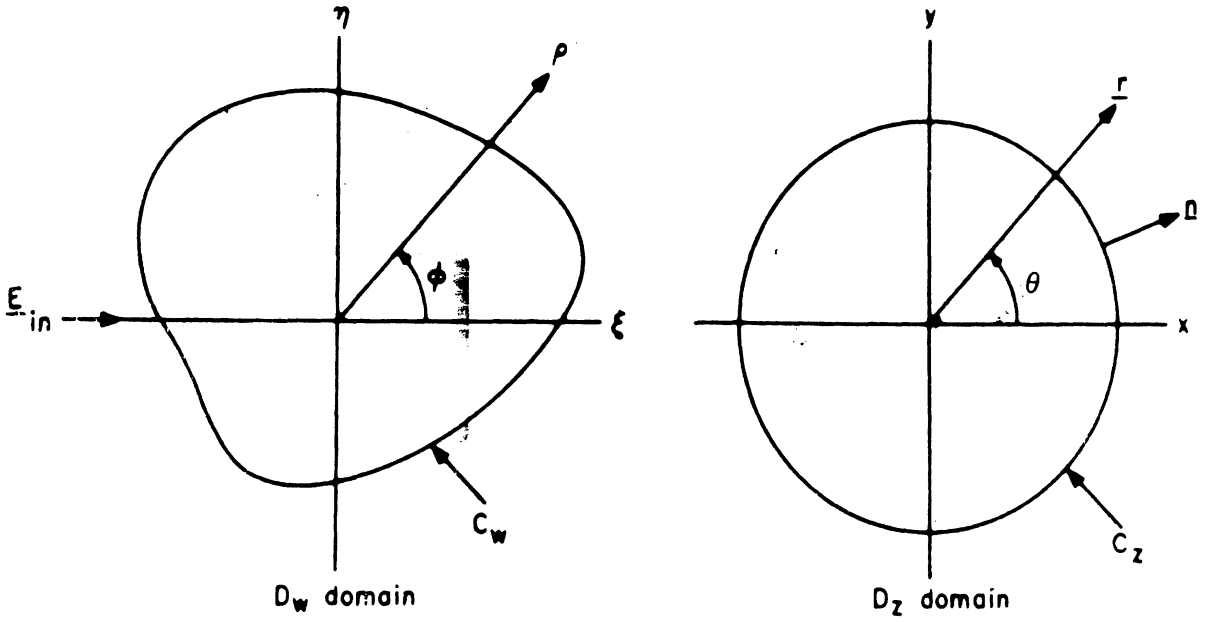

FIG. 2.1: THE MAPPING OF THE BOUNDARY

The scattered field $\underline{E}_s$ must satisfy the Maxwell equations,

$$\nabla \times \underline{E}_s = i\omega\mu_o \underline{H}_s , \qquad \nabla \times \underline{H}_s = -i\omega\epsilon_o \underline{E}_s , \tag{2.1}$$

Sommerfeld's radiation condition and the boundary condition

$$\hat{n} \times (\underline{E}_{in} + \underline{E}_s) = 0 \qquad \text{on the boundary } C_w . \tag{2.2}$$

Here ϵ_o and μ_o are the permittivity and the permeability of free space, respectively.

In the polar coordinate system Eqs. (2.1) and (2.2) can be reduced to scalar forms in terms of the z component of the scattered field $\underline{E}_s$

$$E_{sz} = \tilde{u} \tag{2.3}$$

$$\frac{1}{\rho}\frac{\partial \tilde{u}}{\partial \rho} = i\omega\mu_o H_{s\rho}, \quad \frac{\partial \tilde{u}}{\partial \rho} = -i\omega\mu_o H_{s\phi}$$

$$H_{sz} = E_{s\rho} = E_{s\phi} = 0 , \tag{2.4}$$

and u is the solution of the following boundary value problem;

$$\frac{\partial^2 \tilde{u}}{\partial \rho^2} + \frac{1}{\rho}\frac{\partial \tilde{u}}{\partial \rho} + \frac{1}{\rho^2}\frac{\partial^2 \tilde{u}}{\partial \phi^2} + k^2 \tilde{u} = 0 \qquad \text{in } D_w \tag{2.5}$$

$$\tilde{u} = -e^{ik\xi} \qquad \text{on } C_w \tag{2.6}$$

$$\lim_{\rho \to \infty} \rho^{1/2}\left[\frac{\partial \tilde{u}}{\partial \rho} - ik\tilde{u}\right] = 0 \tag{2.7}$$

where $k = \omega\sqrt{\mu_o \epsilon_o}$ is the wave number.

Up to this point the derivation of the equations has been straightforward involving merely the substitution of terms. However, the solution of this boundary

value problem with an arbitrary shape of the boundary cannot be obtained by the conventional method of separation of variables.

As an alternate approach, let us conformally map the domain external to C_w into another domain where the Green's function satisfying the prescribed boundary condition is known. The point at infinity in the original domain is mapped into the point at infinity in the transformed domain, and the transformed boundary is assumed to be an analytic contour (that is, an infinitely differentiable contour). The transformed domain and boundary are denoted as D_z and C_z respectively (see Fig. 2.1), and the mapping function as $F(z)$.

If the original boundary C_w is a closed piecewise-smooth contour, then the mapping function $F(z)$ is a single valued function everywhere including the boundary C_z, and has isolated singularities at all points on the boundary corresponding to geometrical singularities of C_w (e.g. kinks, or discontinuities in curvature or in its derivatives). Furthermore, the order of singularity of the mapping function is determined by the behavior of the geometry of the original boundary (the scattering body). For more details on properties of the mapping function, the reader is referred to the works done by Nehari[25] and Warschawski[24]

Since the point at infinity in D_w is conformally mapped into the point at infinity in D_z, the mapping function behaves as

$$w = F(z) = z + O(\frac{1}{z}) \qquad \text{as} \quad z \longrightarrow \infty \ . \tag{2.8}$$

Set

$$u(z) = \tilde{u}\left\{F(z)\right\}. \tag{2.9}$$

Then, $u(z)$ satisfies the transformed wave equation and the transformed boundary condition. Since $w \simeq z$ as $z \to \infty$ (see Eq. (2.8)), the radiation condition is invariant. Therefore, the original boundary value problem of Eqs. (2.5), (2.6) and (2.7) is transformed into

$$\frac{\partial^2 u}{\partial r^2} + \frac{1}{r}\frac{\partial u}{\partial r} + \frac{1}{r^2}\frac{\partial^2 u}{\partial \theta^2} + k^2 \left|\frac{dw}{dz}\right|^2 u = 0 \quad \text{in } D_z , \tag{2.10}$$

$$u = -e^{ik\,\mathrm{Re}\,F(z)} \quad \text{on } C_z , \tag{2.11}$$

$$\lim_{r\to\infty} r^{1/2}\left[\frac{\partial u}{\partial r} - iku\right] = 0 . \tag{2.12}$$

Once we obtain the solution $u(z)$ of the transformed boundary value problem, the far field expression of $\tilde{u}(w)$ can be easily obtained since the mapping function becomes an identity as $z \to \infty$.

2.2 Remarks on the Transformed Equations

The transformed boundary value problem of Eqs. (2.10), (2.11) and (2.12) is mathematically the same as the problem of radiation from a cylinder in an inhomogeneous medium.

The transformed boundary value, $-\exp\{ik\,\mathrm{Re}\,F(z)\}$, introduces an equivalent source on the new boundary C_z. The behavior of $F(z)$ on the boundary is determined by that of the geometry of the original boundary. This property will be used in Chapter 4 to study effects of a geometrical singularity of the scattering body in high frequency scattering.

The transformed wave equation introduces an inhomogeneity $\left|\frac{dw}{dz}\right|$ in the medium. In case of k=0 (Laplace's equation), the effects of inhomogeneity in the medium disappears. The role of $\left|\frac{dw}{dz}\right|$ for $k \neq 0$ (the wave equation) can be effectively demonstrated in terms of the theory of ray tracing. This theory is concerned with the asymptotic solution of the wave equation in case of $k\left|\frac{dw}{dz}\right| >> 1$.

Under conformal mapping, the following three phenomena can be observed:

a) The optical length is invariant

$$L_w \equiv \int |dw| = \int \left|\frac{dw}{dz}\right| |dz| \equiv L_z$$

b) The amplitude of ray is invariant

The amplitude of ray in the original domain is inversely proportional to the linear distance Δ_w between two adjacent rays. In the transformed domain the amplitude of ray is inversely proportional to $\left|\frac{dw}{dz}\right| \Delta_z$ where Δ_z is the linear distance between two adjacent rays in the transformed domain.

Since

$$\Delta_w = \left|\frac{dw}{dz}\right| \Delta_z ,$$

the amplitude of ray is invariant under conformal mapping.

c) Curvature

The two curvatures $\frac{1}{R_w}$ of the contour C_w and $\frac{1}{R_z}$ of C_z are related by

$$\frac{1}{R_w} = \frac{1}{\left|\frac{dw}{dz}\right|}\left[\frac{1}{R_z} - \hat{n}\cdot\nabla \mathrm{Log}\left|\frac{dw}{dz}\right|\right]. \qquad (2.13)$$

In Eq. (2.13)

$$\hat{n}\cdot\nabla \mathrm{Log}\left|\frac{dw}{dz}\right| = \frac{1}{R_{ray}} \qquad (2.14)$$

is the curvature of the ray bent by the inhomogeneity $\left|\frac{dw}{dz}\right|$. Therefore, by means of conformal mapping, the curvature of the boundary C_w is decomposed into the curvature of the new boundary C_z and the curvature of the ray.

These three properties were first observed by Jones[22]. He derived an asymptotic solution of Eq. (2.10) in the case $k\left|\frac{dw}{dz}\right| >> 1$ by the W.K.B.J.L. method, and this solution was shown to be invariant under conformal mapping because of the three properties discussed above. For details of Jones' work, the reader is referred to his paper[22].

The properties a, b and c fail when the mapping function is not conformal. Therefore, Jones' method is not applicable when the boundary has a kink or a discontinuity in curvature. To handle such geometrical irregularities of the boundary in scattering problems, an integral equation method is developed in the following section.

2.3 Integral Representation and the Solution

In this section Garabedian's integral equation is derived and its solution is discussed.

Green's function $G(\underline{r}_1, \underline{r})$ in the D_z domain, satisfying the Dirichlet boundary condition, is defined by the following three equations:

$$\nabla^2 G + k^2 G = -\delta(|\underline{r}_1 - \underline{r}|) \qquad \text{in } D_z$$

$$G = 0 \qquad \text{on } C_z \qquad (2.15)$$

$$\lim_{r \to \infty} r^{1/2} \left[\frac{\partial G}{\partial r} - ikG\right] = 0$$

Once Green's function is known, $u(z)$, which satisfies Eqs. (2.10), (2.11) and (2.12), can be represented as an integral equation by Green's theorem.

$$u(\underline{r}_1) = -\oint_{C_z} \frac{\partial G(\underline{r}_1, \underline{r})}{\partial n} \exp\left\{ik R_e F(z)\right\} d\ell + \iint_{D_z} G(\underline{r}_1, \underline{r}) \left(\left|\frac{dw}{dz}\right|^2 - 1\right) u(\underline{r}) k^2 dxdy \qquad (2.16)$$

This is Garabedian's integral equation. The first term in the right-hand side of Eq. (2.16) is known. The kernel $G(\underline{r}_1, \underline{r}) \cdot \left\{\left|\frac{dw}{dz}\right|^2 - 1\right\}$ of this equation is of order $r^{-5/2}$ as $r \to \infty$, and is bounded everywhere except at the point $\underline{r} = \underline{r}_1$ where the Green's function has a logarithmic singularity. So Eq. (2.16) is a Fredholm integral equation of the second kind.

It is interesting to note that the first (known) term of Eq. (2.16) satisfies the inhomogeneous Dirichlet boundary condition given by Eq. (2.11). Neglecting the effects of inhomogeneity $\left|\frac{dw}{dz}\right|$, this term can be interpreted physically as a field radiated from C_z, due to the source given by the transformed boundary value. The second term of Eq. (2.16), on the other hand, satisfies an homogeneous Dirichlet boundary condition, and represents the effects of inhomogeneity $\left|\frac{dw}{dz}\right|$ in the medium on the propagation of the radiated and scattered fields.

Eq. (2.16) can be solved by a successive approximation, provided that the iterated series (the Neumann series) converges. Let us discuss the conditions

of convergence in L^2 space (for more detail, the reader is referred to Mikhlin's book[26]). The inhomogeneous term of Eq. (2.16) is square integrable in the D_z domain if this term is multiplied by the factor $(kr_1)^{-1}$.

$$\frac{u(\underline{r}_1)}{kr_1} = -\oint_{C_z} \frac{1}{kr_1} \frac{\partial G(\underline{r}_1, \underline{r})}{\partial n} \cdot \exp\left\{ikRe F(z)\right\} d\ell + \int\int_{D_z} \tilde{K}(\underline{r}_1, \underline{r}) \frac{u(r)}{kr} k^2 dxdy \tag{2.17}$$

where

$$\tilde{K}(\underline{r}_1, \underline{r}) = \left(\left|\frac{dw}{dz}\right|^2 - 1\right) (kr)^2 \frac{G(\underline{r}_1, \underline{r})}{k^2 r_1 r} . \tag{2.18}$$

The Neumann series solution of Eq. (2.17) converges if

$$\left\|\tilde{K}\right\|^2 = \int\int_{D_{z_1}} \int\int_{D_z} \left|\tilde{K}^2(\underline{r}_1, \underline{r})\right| k^2 dxdy\, k^2 dx_1 dy_1 < 1 . \tag{2.19}$$

When C_w is geometrically similar to C_z such that

$$\left|r_w(\theta) - r_z(\theta)\right| \leq \delta \qquad \text{for all } 0 \leq \theta < 2\pi \tag{2.20}$$

where r_z (or r_w) is a polar coordinate representing C_z (or C_w), then $\left|F(z) - z\right|$ is of order δ for a small δ. Furthermore, if C_w has continuous tangents everywhere (no kinks), then $\left|\left|\frac{dw}{dz}\right|^2 - 1\right|$ times the characteristic dimension of C_z is also of order δ (Warschawski[27]). Let the mapping function given by Eq. (2.8) be rewritten as

$$w = F(z) = z + \delta f(z) \tag{2.21}$$

where $f(z)$ is a dimensionless quantity.

Then Eq. (2.18) becomes

$$\tilde{K}(\underline{r}_1, \underline{r}) = k\delta\left(\frac{2}{k}\,\mathrm{Re}\,f'(z) + \frac{\delta}{k}\,|f'(z)|^2\right)\cdot (kr)^2\,\frac{G(\underline{r}_1, \underline{r})}{k^2 r_1 r}\quad , \tag{2.22}$$

and $\|\tilde{K}\|$ is of order $k\delta$ for a small $k\delta$.

If $k\delta$ is sufficiently small such that Eq. (2.19) is true, then the solution of Garabedian's integral equation is given by the Neumann series:

$$\frac{u(\underline{r}_1)}{kr_1} = \frac{u_o(\underline{r}_1)}{kr_1} + \sum_{n=1}^{\infty}\iint_{D_z} \tilde{K}_n(\underline{r}_1, \underline{r})\,\frac{u_o(r)}{kr}\,k^2\,dxdy \tag{2.23}$$

where

$$u_o(\underline{r}_1) = -\oint_{C_z} \frac{\partial G(\underline{r}_1, \underline{r})}{\partial n}\cdot \exp\left\{ik\,\mathrm{Re}\,F(z)\right\}\,d\ell \tag{2.24}$$

and $\tilde{K}_n(\underline{r}_1, \underline{r})$ is determined by the recurrence relationship,

$$\tilde{K}_1(\underline{r}_1, \underline{r}) = \tilde{K}(\underline{r}_1, r)\,; \quad \tilde{K}_n(\underline{r}_1, \underline{r}) = \iint_{D_z} \tilde{K}(\underline{r}_1, \underline{r}')\tilde{K}_{n-1}(\underline{r}', \underline{r})k^2\,dx'dy'. \tag{2.25}$$

$\tilde{K}_n(\underline{r}_1, \underline{r})$ is called the n-th iterated kernel.

CHAPTER III

SCATTERING OF A PLANE WAVE BY AN ALMOST CIRCULAR CYLINDER

For a specific example of the conformal mapping method, the scattering of a plane wave by an almost circular cylinder with periodic, smooth and shallow corrugations is studied. Later this result is compared with that of Clemmow and Weston[28].

3.1 The Mapping Function

In this section, a simple method of obtaining the function conformally mapping an almost circular domain into a circular domain is briefly discussed without proof. Details of this method can be found in the books by Nehari[25] or Kantorovich and Krylov[29].

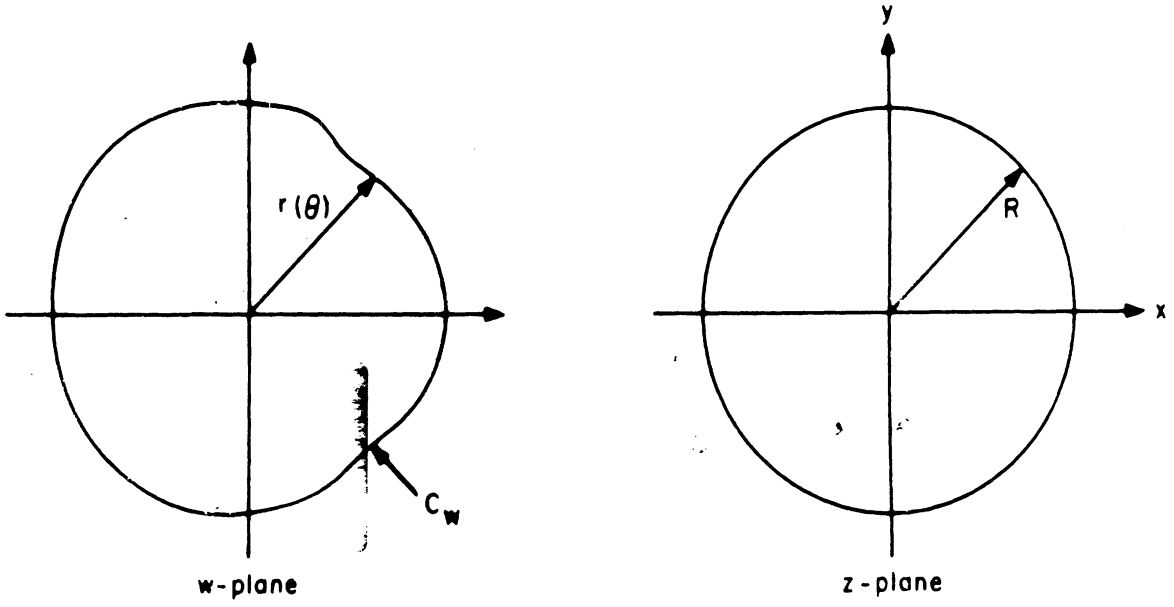

FIG. 3.1: MAPPING OF AN ALMOST CIRCULAR DOMAIN

Let the given almost circular boundary C_w be represented by the polar equation

$$r(\theta) = R + r_p(\theta) , \tag{3.1}$$

and assume that $r_p(\theta)$ is piecewise continuous, bounded such that

$$\left| r_p(\theta) \right| \leq \delta << 1 . \tag{3.2}$$

$r_p(\theta)$ is represented by a Fourier series;

$$r_p(\theta) = \sum_{n=1}^{\infty} (a_n \cos n\theta + b_n \sin n\theta) . \tag{3.3}$$

In this case, the mapping function, which maps the domain D_z exterior to a circle C_z into a domain D_w exterior to C_w, is given by

$$w = F(z) = z + \sum_{n=1}^{\infty} \frac{a_n + i b_n}{\left(\frac{z}{R}\right)^{n-1}} + O(\delta^2) . \tag{3.4}$$

On the boundary $|z| = R$, the real part of the mapping function is given by the closed form;

$$\mathrm{Re}\, F(z) \cong R\cos\theta + \left[\cos\theta \cdot r_p(\theta) - \sin\theta \cdot \bar{r}_p(\theta) \right] \tag{3.5}$$

where

$$\bar{r}_p(\theta) = \frac{1}{2\pi} \, \mathrm{P.V.} \int_0^{2\pi} r_p(t) \cot \frac{t-\theta}{2} \, dt .$$

3.2 Scattering by an Almost Circular Cylinder

As an example of application of the conformal mapping method, the scattering problem of a plane wave by an almost circular cylinder with periodic, smooth and shallow corrugations is considered.

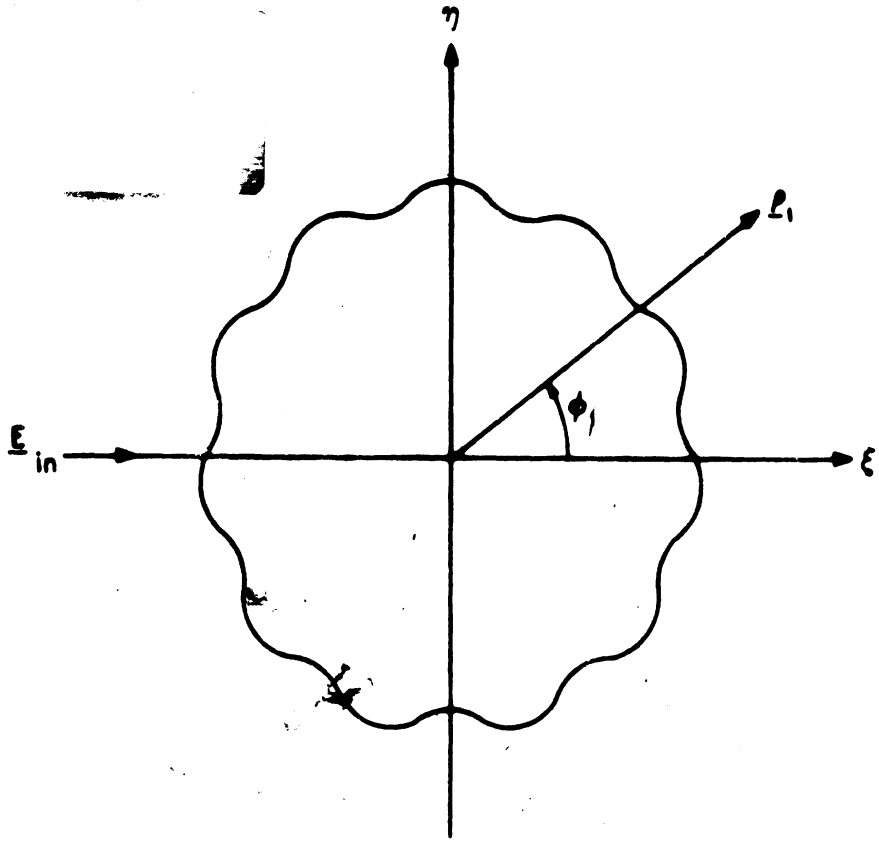

FIG. 3.2: AN ALMOST CIRCULAR CYLINDER WITH PERIODIC, SMOOTH AND SHALLOW CORRUGATIONS

Let the boundary C_w of the scattering body be represented as

$$r = R + a\cos\ell\theta + b\sin\ell\theta \tag{3.6}$$

(note that for $\ell = 2$, C_w is an elliptic cylinder). Here the perturbation factor

$$k\delta = k\sqrt{a^2+b^2} \tag{3.7}$$

is assumed to be sufficiently small such that both $k\delta$ and the norm of the kernel of Garabedian's integral equation (see Eq. (2.19)) is much smaller than unity. Then neglecting $(k\delta)^2$ and higher order terms, the transformed field $u(\underline{r}_1)$ is given by the first and a part of the second term of the Neumann series

of Eq. (2.23).

$$u(\underline{r}_1) = u_{circle}(\underline{r}_1) + u_{p_1}(\underline{r}_1) + u_{p_2}(\underline{r}_1) + O(k\delta)^2 \tag{3.8}$$

where

$$u_{circle}(\underline{r}_1) = -\int_{r=R} \exp\left\{ikR\cos\theta\right\} \cdot \frac{\partial G(\underline{r}_1, \underline{r})}{\partial r} R\, d\theta \tag{3.9}$$

$$u_{p_1}(\underline{r}_1) = -\int_{r=R} ik\left[a\cos(\ell-1)\theta + b\sin(\ell-1)\theta\right] \exp(ikR\cos\theta) \cdot \frac{\partial G(\underline{r}_1, \underline{r})}{\partial r} R\, d\theta \tag{3.10}$$

$$u_{p_2}(\underline{r}_1) = 2\iint_{|z|>R} G(\underline{r}_1, \underline{r}) \cdot \mathrm{Re}\left[\left(\frac{dw}{dz} - 1\right)\right] \cdot u_{circle}(\underline{r})\, k^2\, dxdy \tag{3.11}$$

and

$$G(\underline{r}_1, \underline{r}) = \frac{i}{4} \sum_{n=-\infty}^{\infty} e^{in(\theta_1 - \theta)} H_n^{(1)}(kr_1)\left[J_n(kr) - \frac{J_n(kR)}{H_n^{(1)}(kR)} H_n^{(1)}(kr)\right] \tag{3.12}$$

for $r_1 > r$.

Substituting the expansion form of $e^{ikR\cos\theta}$ (Magnus and Oberhettinger[30]), viz.

$$\exp\left\{ikR\cos\theta\right\} = \sum_{n=-\infty}^{\infty} i^n e^{in\theta} J_n(kR) ,$$

and Eq. (3.12) into (3.9), u_{circle} is given by

$$u_{circle}(\underline{r}_1) = -\sum_{n=-\infty}^{\infty} i^n e^{in\theta_1} \frac{J_n(kR)}{H_n^{(1)}(kR)} H_n^{(1)}(kr_1) . \tag{3.13}$$

u_{circle} is the field resulting from the scattering of a plane wave by a circular cylinder of radius R. $u_{p_1}(\underline{r}_1)$ can be obtained by a similar method, viz.

$$u_{p_1}(\underline{r}_1) = -\frac{1}{2}\sum_{n=-\infty}^{\infty} i^n e^{in\theta_1} \frac{H_n^{(1)}(kr_1)}{H_n^{(1)}(kR)} \left[i^{\ell} k(a+ib) J_{n+\ell-1}(kR) \right.$$

$$\left. -i^{-\ell} k(a-ib) \cdot J_{n-\ell+1}(kR) \right]. \qquad (3.14)$$

u_{p_2} can be evaluated by substituting Eqs. (3.4), (3.13) into (3.11) and using the following integral formula

$$\int_0^{R_1} R^{\mu+r+1} C_\mu(R) D_r(R) dR = \frac{R_1^{\mu+r+1}}{2(\mu+r+1)} \left[C_\mu(R_1) D_r(R_1) + C_{\mu+1}(R_1) D_{r+1}(R_1) \right], \qquad (3.15)$$

where C and D are any cylindrical functions. Thus

$$u_{p_2}(\underline{r}_1) \simeq \frac{i}{4}\sqrt{\frac{2}{\pi k r_1}}\, e^{ikr_1 - i\frac{\pi}{4}} \sum_{n=-\infty}^{\infty} \frac{e^{in\theta_1}}{H_n^{(1)}(kR)} \left[i^{\ell} \frac{k(a+ib)}{2} \right.$$

$$\left. J_{n+\ell}(kR) \frac{H_{n+\ell-1}^{(1)}(kR)}{H_{n+\ell}^{(1)}(kR)} - i^{-\ell} \frac{k(a-ib)}{2} J_{n-\ell}(kR) \frac{H_{n-\ell+1}^{(1)}(kR)}{H_{n-\ell}^{(1)}(kR)} \right]. \qquad (3.16)$$

u_{p_1} and u_{p_2} represent the perturbed field. Using the relationship (see Magnus and Oberhettinger[30]).

$$J_{n-1}(z)H_n^{(1)}(z) - J_n(z)H_{n-1}^{(1)}(z) = \frac{2}{\pi i z}, \qquad (3.17)$$

the sum of u_{p_1} and u_{p_2} is given as

$$u_p = u_{p_1} + u_{p_2} \simeq \sqrt{\frac{2}{\pi k r_1}}\, e^{ikr_1 - i\frac{\pi}{4}} \sum_{n=-\infty}^{\infty} \frac{e^{in\theta_1}}{H_n^{(1)}(kR)}$$

$$\left[i^{\ell} \cdot \frac{k(a+ib)}{2} \left\{ -J_{n+\ell-1}(kR) + J_{n+\ell}(kR) \frac{H_{n+\ell-1}^{(1)}(kR)}{H_{n+\ell}^{(1)}(kR)} \right\} \right.$$

$$\left. + i^{-\ell} \cdot \frac{k(a-ib)}{2} \left\{ -J_{n-\ell}(kR) \frac{H_{n-\ell+1}^{(1)}(kR)}{H_{n-\ell}^{(1)}(kR)} + J_{n-\ell+1}(kR) \right\} \right]$$

$$= \sqrt{\frac{2}{\pi k r_1}}\, e^{ikr_1 + i\frac{\pi}{4}} \cdot \frac{1}{\pi} \sum_{n=-\infty}^{\infty} \frac{e^{in\theta_1}}{H_n^{(1)}(kR)} \left[i^{\ell} \frac{(a+ib)/R}{H_{n+\ell}^{(1)}(kR)} \right.$$

$$\left. + i^{-\ell} \cdot \frac{(a-ib)/R}{H_{n-\ell}^{(1)}(kR)} \right] . \qquad (3.18)$$

Since $F(z)$ of Eq. (3.4) $\longrightarrow z$ as $z \to \infty$, the mapping function becomes an identity for the far field. Therefore, the far field scattered by an almost circular cylinder with periodic, smooth and shallow corrugations is given by

$$\tilde{u}(\underline{\rho}_1) = \tilde{u}_{\text{circle}}(\underline{\rho}_1) + \tilde{u}_p(\underline{\rho}_1) + O(k\delta)^2 \qquad (3.19)$$

where $\tilde{u}_{\text{circle}}$ is the scattered field of a plane wave by a circular cylinder of radius R, and $\tilde{u}_p(\underline{\rho}_1)$ is the perturbed field given by

$$\tilde{u}_p(\underline{\rho}_1) \simeq \sqrt{\frac{2}{\pi k \rho_1}}\, e^{ik\rho_1 + i\frac{\pi}{4}} \frac{1}{\pi} \sum_{n=-\infty}^{\infty} \frac{e^{in\phi_1}}{H_n^{(1)}(kR)} \left[i^{\ell} \frac{(a+ib)/R}{H_{n+\ell}^{(1)}(kR)} \right.$$

$$\left. + i^{-\ell} \frac{(a-ib)/R}{H_{n-\ell}^{(1)}(kR)} \right] . \qquad (3.20)$$

The solution in Eq. (3.19) agrees with the result of Clemmow and Weston[28] who obtained the same solution by means of a perturbation and Fourier transform method, and they also obtained the asymptotic form of $u_p(\rho_1)$ for $kR \gg 1$. In their original paper, the discussion about the limit of validity of the solution (3.19) was based on physical interpretation of the solution. But from the study of the iterated solution of the integral equation (2.33), it is now clear that the conditions for validity of the solution of (3.19) are not only $k\delta \ll 1$ but also $||\tilde{K}|| \ll 1$ as given by Eq. (2.19).

CHAPTER IV

EFFECTS OF EDGES IN HIGH FREQUENCY SCATTERING

In this chapter, the problem of diffraction by edges with discontinuities in curvature or in its derivatives is handled by the conformal mapping method. It is found that the dominant contribution of the edge-effects on diffracted fields is given in the form of a contour integral. The behavior of the mapping function near the edge, necessary for the evaluation of the contour integral, is discussed in Section 4.2.

4.1 Integral Representation of Effects of Edges

When a wave hits an edge, the incident ray produces infinitely many diffracted rays (Keller[31]). This kind of diffraction problem can be handled by the integral equation method derived in Chapter 2.

As a first step, the given boundary with a finite number of edges is mapped into a new boundary which is free of edges. The transformed function of the scattered field, $u(\underline{r}_1)$, is then given as a solution of Garabedian's integral equation. This equation is derived in Chapter 2 and is given as

$$\frac{u(\underline{r}_1)}{kr_1} = \frac{u_o(\underline{r}_1)}{kr_1} + \iint_{D_z} \tilde{K}(\underline{r}_1, \underline{r}) \frac{u(\underline{r})}{kr} k^2 dxdy \qquad (4.1)$$

where

$$u_o(\underline{r}_1) = - \oint_{C_z} \exp ik \left\{ x + \delta \operatorname{Re} f(z) \right\} \frac{\partial G(\underline{r}, \underline{r}_1)}{\partial n} d\ell \,. \qquad (4.2)$$

The kernel function $\tilde{K}$ is given by Eq. (2.22) as

$$\tilde{K}(\underline{r}_1, \underline{r}) = k\delta \left\{ \frac{2}{k} \mathrm{Re}\, f'(z) + \frac{\delta}{k} \left| f'(z) \right|^2 \right\} (kr)^2 \frac{G(\underline{r}_1, \underline{r})}{k^2 r_1 r} , \qquad (4.3)$$

and δ in the above equation is defined by Eq. (2.20) as the maximum linear distance between the original and the transformed boundaries.

It is shown in Section 2.3 that Eq. (4.1) can be solved by a successive approximation method, provided that $k\delta$ is sufficiently small so that

$$\| \tilde{K} \| < 1 \quad \text{(see Eq. (2.19))}.$$

At least in principle, $k\delta$ can be chosen arbitrarily small. Formally, this can be accomplished in the following way. Choose the transformed boundary C_z as identical to the original boundary C_w except near the edge, where C_w is perturbed so that $k\delta$ is as small as desired. In certain cases, by perturbing the original boundary, the new boundary may have points of discontinuity in derivatives of higher order than that of the edge of C_w. It will be shown later (Chapter 6) that the effect of a discontinuity in the n-th derivative of the tangent on the diffracted field is of order $k^{-n}(k\rho_1)^{-1/2}$. Therefore, the effect of the new discontinuity in the higher order derivative of the tangent may be neglected compared to the effect of the original edge of the scattering body.

Unfortunately for given C_z and C_w, a simple local mapping function near the edge is not available. Therefore at the present state, it is assumed that the boundary of the scattering body is almost circular. Then map C_w into a circle C_z and use the technique of Section 3.1 to obtain the desired mapping function approximately.

The norm of $\tilde{K}$ in Eq. (4.1) is of order $k\delta$ and can be much smaller than unity for a sufficiently small $k\delta$ (see Section 2.3). Then the solution of Eq. (4.1) can be obtained by a successive approximation method. We now examine the first (known) term in Eq. (2.23) when the wavelength of the incident wave is small compared to the minimum radius of curvature of the scattering body.

In order to examine the asymptotic behavior of the first term $u_o(\underline{r}_1)$ for high frequencies, it is convenient to use the asymptotic form of $\frac{\partial G}{\partial n}$ derived in Appendix A, viz.

$$\left.\frac{\partial G(\underline{r}_1, \underline{r})}{\partial r}\right|_{r=R} \simeq \sqrt{\frac{2}{\pi k r_1}}\, e^{ikr_1 - i\frac{\pi}{4}} \cdot \frac{ik}{4M}$$

$$\cdot \sum_{n=0}^{\infty} \left[\tilde{f}(\zeta_n) \exp\left\{ ikR(-\theta_1 + \theta - \frac{\pi}{2} + 2n\pi) \right\} \right.$$

$$\left. + \tilde{f}(\zeta_n') \exp\left\{ ikR(\theta_1 - \theta + \frac{3}{2}\pi + 2n\pi) \right\} \right]$$

$$\text{for } kR \gg 1 , \tag{4.4}$$

where

$$M = \left(\frac{kR}{2}\right)^{1/3}$$

$$\zeta_n = (-\theta_1 + \theta - \frac{\pi}{2} + 2n\pi)M$$

$$\zeta_n' = (\theta_1 - \theta + \frac{3\pi}{2} + 2n\pi)M \tag{4.5}$$

and

$$\tilde{f}(\zeta) = \frac{1}{\sqrt{\pi}} \int_{\Gamma} \frac{e^{i\zeta t}}{w_1(t)}\, dt . \tag{4.6}$$

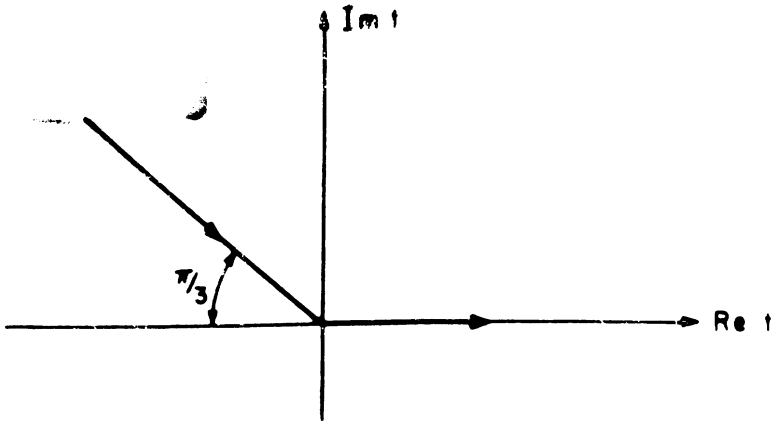

FIG. 4.1: THE Γ CONTOUR

$w_1(t) = \sqrt{\pi}\left[Bi(t) + iAi(t)\right]$ is an Airy function, and $\tilde{f}(\zeta)$ is the Fock function[4].

Using the asymptotic form of Green's function, an approximate expression of $u_o(\underline{r}_1)$ can be obtained by direct substitution of Eq. (4.4) into (4.2).

$$u_o(\underline{r}_1) \simeq \sqrt{\frac{2}{\pi k r_1}}\, e^{ikr_1 - i\frac{\pi}{4}} \left[\tilde{\sigma} + \tilde{\sigma}^*\right] + O(k\delta)^2 \tag{4.7}$$

where

$$\tilde{\sigma} = i\frac{M^2}{2}\int_{-\infty}^{\pi} d\theta \left[1 + g(-\theta+\pi+\theta_1)\right] \exp\left\{ikR\left(-\cos(\theta_1-\theta) - \theta + \frac{\pi}{2}\right)\right\} \tilde{f}\left\{\zeta = M\left(\frac{\pi}{2} - \theta\right)\right\} \tag{4.8}$$

$$\tilde{\sigma}^* = i\frac{M^2}{2}\int_{-\pi}^{\infty} d\theta \left[1 + g(-\theta+\pi+\theta_1)\right] \exp\left\{ikR\left(-\cos(\theta_1-\theta) + \theta + \frac{\pi}{2}\right)\right\} \tilde{f}\left\{\zeta = M\left(\frac{\pi}{2} + \theta\right)\right\} \tag{4.9}$$

and

$$g(\theta) \equiv ik\delta\, \mathrm{Re}\, f(\mathrm{Re}^{i\theta} = z) \tag{4.10}$$

is related to the real part of the mapping function on the boundary (see Eq. (2. 21)).

For $kR \gg 1$, the contour integrals of $\tilde{\sigma}$ and $\tilde{\sigma}^*$ can be asymptotically evaluated by the saddle point method (Vander Waerden[32]). Set

$$\tilde{v} = -ikR\left[-\cos(\theta_1 - \theta) + \frac{\pi}{2} - \theta\right] \tag{4.11a}$$

and

$$\tilde{v}^* = -ikR\left[-\cos(\theta_1 - \theta) + \frac{\pi}{2} + \theta\right]. \tag{4.11b}$$

By Eqs. (4. 11a and b), Eqs. (4. 8) and (4. 9) can be rewritten as

$$\tilde{\sigma} = -i\frac{M^2}{2}\int_{\tilde{v}(\theta=\pi)}^{-i\infty} d\tilde{v}\, e^{-\tilde{v}}\frac{d\theta}{d\tilde{v}}\left[1 + g(-\theta+\pi+\theta_1)\right]\cdot \tilde{f}\left\{\xi = M(\frac{\pi}{2} - \theta)\right\} \tag{4.12}$$

and

$$\tilde{\sigma}^* = -i\frac{M^2}{2}\int_{\tilde{v}^*(\theta=-\pi)}^{-i\infty} d\tilde{v}^*\, e^{-\tilde{v}^*}\frac{d\theta}{d\tilde{v}^*}\left[1 + g(-\theta+\pi+\theta_1)\right]\cdot \tilde{f}\left\{\xi = M(\frac{\pi}{2} + \theta)\right\}. \tag{4.13}$$

In the $\tilde{v}$ (or $\tilde{v}^*$) plane, the integrand of Eq. (4. 12) (or (4. 13)) has two kinds of branch points; one is due to the saddle points $\left(\frac{d\tilde{v}}{d\theta} = 0 \text{ or } \frac{d\tilde{v}^*}{d\theta} = 0\right)$, and the other to the branch points of $g(\theta)$. The branch points of $g(\theta)$ are in turn due to the geometrical singularity of the surface of the scattering body.

By choosing branch cuts parallel to the real axis in $\tilde{v}$(or $\tilde{v}^*$) plane and deforming the contour of integration, $\tilde{\sigma}$(or $\tilde{\sigma}^*$) can be written as a sum of branch cut integrals. Branch cut integrals due to the saddle points represent the specularly reflected field and the fields diffracted by the shadow boundary (see Appendix B and Goriainov's paper[9]). The branch cut integrals due to singularities of $g(\theta)$ represent the effects of an edge of the scattering

body in the first term of the Neumann series. These various sources of the scattered and diffracted fields are in agreement with the predictions of the geometrical theory of diffraction (see Keller's paper[31]).

As discussed in Chapter 2, the iterated terms in the Neumann series represent corrections to the diffracted fields due to the change of the ray paths under the conformal transformation. We now consider only the fields diffracted by the edge, and postpone the discussion of corrections arising from the iterated terms until Chapter 6. Then the fields diffracted by an edge are given as

$$\tilde{u}_d(\rho) \simeq \sqrt{\frac{2}{\pi k \rho_1}}\, e^{ik\rho_1 - i\frac{\pi}{4}} \left[\sigma + \sigma^*\right] + O(k\delta)^2 \tag{4.14}$$

where

$$\sigma = -i\frac{M^2}{2} \int_{C_d} d\tilde{v}\, e^{-\tilde{v}} \frac{d\theta}{d\tilde{v}} \cdot g(-\theta + \phi_1 + \pi) \cdot \tilde{f}\left\{\zeta = M(\tfrac{\pi}{2} - \theta)\right\} \tag{4.15}$$

$$\sigma^* = i\frac{M^2}{2} \int_{C_d^*} d\tilde{v}^*\, e^{-\tilde{v}^*} \frac{d\theta}{d\tilde{v}^*} \cdot g(-\theta + \phi_1 + \pi) \cdot \tilde{f}\left\{\zeta = M(\tfrac{\pi}{2} + \theta)\right\}, \tag{4.16}$$

and C_d and C_d^* are branch cut contours due to the branch points of $g(\theta)$.

Equations (4.15) and (4.16) can be evaluated once the function $g(\theta)$ is known. $g(\theta)/ik$ is the real part of $F(z) - z$ on the boundary, and it will be investigated in the next section.

The Fock functions $\tilde{f}(\zeta)$ in Eqs. (4.15) and (4.16) represent physically the current induced on the circular cylinder by the incident plane wave (see Goodrich[10]). $\tilde{f}(\zeta)$ admits an expansion in a series of residues for $\zeta > 0$.

$$\tilde{f}(\zeta) = 2\sqrt{\pi}\, i \sum_{s=1}^{\infty} \frac{e^{i\zeta t_s}}{w_1'(t_s)} , \tag{4.17}$$

where t_s is the s-th root of $w_1(t)$ and numerical values of t_s are given in various papers (e.g. Fock's paper[3]). For a large ζ, $\tilde{f}(\zeta)$ has the following asymptotic behavior:

$$e^{i\frac{\zeta^3}{3}} \tilde{f}(\zeta) = 2i\zeta \qquad \text{as } \zeta \longrightarrow -\infty \tag{4.18}$$

$$= 0 \qquad \text{as } \zeta \longrightarrow \infty \tag{4.19}$$

The expansion form of the residue series Eq. (4.17) represents diffracted fields in the shadow region and they are called creeping waves. Near shadow boundaries, the following relations hold

$$\text{(a)}\quad kR(\frac{\pi}{2} - \theta) \simeq kR\cos\theta + \frac{M^3}{3}(\frac{\pi}{2} - \theta)^3 \qquad \text{for } \theta \simeq \frac{\pi}{2}$$

$$\text{(b)}\quad kR(\frac{\pi}{2} + \theta) \simeq kR\cos\theta + \frac{M^3}{3}(\frac{\pi}{2} + \theta)^3 \qquad \text{for } \theta \simeq -\frac{\pi}{2} \ . \tag{4.20}$$

When the argument $\tilde{f}(\zeta)$ has a large negative value, $e^{i\frac{\zeta^3}{3}} \tilde{f}(\zeta)$ becomes a physical optics term by substituting Eq. (4.20) into Eq. (4.18) (see Goriainov's paper[9]). Therefore, in the following chapters $\exp\left\{ikR(\pm\theta + \frac{\pi}{2})\right\} \cdot \tilde{f}\left\{\zeta = M(\pm\theta + \frac{\pi}{2})\right\}$ in Eqs. (4.15) and (4.16) is replaced by its asymptotic form $2iM\cos\theta\, e^{ikR\cos\theta}$ whenever the argument of $\tilde{f}(\zeta)$ has a large negative value.

4.2 Behavior of the Mapping Function Near the Edge

In this section, behavior of the function $g(\theta)$ is examined. $g(\theta)$ is defined by Eq. (4.10) and by Eq. (3.5) as

$$g(\theta) = ik\delta \, \mathrm{Re}\, f(z=Re^{i\theta})$$
$$= ik\left[\cos\theta \cdot r_p(\theta) - \sin\theta \cdot \bar{r}_p(\theta)\right] \qquad (4.21)$$

where

$$\bar{r}_p(\theta) = \frac{1}{2\pi} \, P.V. \int_0^{2\pi} r_p(t) \cdot \cot\frac{t-\theta}{2} \, dt \, .$$

$\bar{r}_p(\theta)$ exists at every point where $r_p(\theta)$ satisfies the Lipshitz condition.

Furthermore, if $r_p(\theta)$ has a discontinuity in the n-th derivative with respect to θ at $\theta=\theta_o$, then $\bar{r}_p(\theta)$ behaves as $(\theta-\theta_o)^{n-1} \mathrm{Log}\,(\theta-\theta_o)^2$ near $\theta=\theta_o$. So the degree of singularity of the function $g(\theta)$ is determined by the degree of singularity of the boundary of the scattering body. For more details, the reader is referred to Warschawski's paper[24]. This property enables us to study the effects of discontinuities in curvature and in its derivatives by means of the integral equation (4.14).

As a specific example, let us consider a convex contour constructed by smoothly joining together a semicircle and a semiellipse.

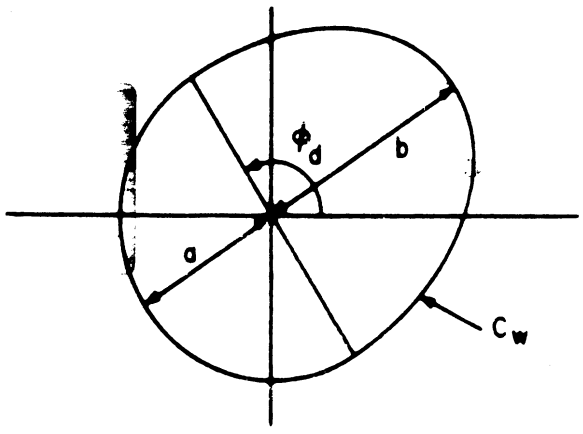

FIG. 4.2: A CONVEX, CLOSED CONTOUR WITH TWO DISCONTINUITIES IN CURVATURE

$$r(\theta) \begin{cases} = a\left\{1-\epsilon^2 \sin^2(\theta-\phi_d)\right\}^{-1/2} \simeq a\left[1+\dfrac{\epsilon^2}{2}\sin^2(\theta-\phi_d)\right] & \text{for } \phi_d-\pi \le \theta \le \phi_d \\ = a & \text{for } \phi_d \le \theta \le \phi_d+\pi \end{cases} \tag{4.22}$$

where $\delta^2 \simeq a^2\epsilon^4$ and higher order terms are assumed to be negligible.

Let us map C_w into a circle with radius R which is given by the following equation

$$R = \frac{1}{2\pi}\int_0^{2\pi} r(\theta)\, d\theta \cong a\left(1+\frac{\epsilon^2}{8}\right) \tag{4.23}$$

Then

$$\begin{aligned} r_p(\theta) \equiv r(\theta) - R &\simeq \frac{\epsilon^2 R}{2}\left[\sin^2(\theta-\phi_d)-\frac{1}{4}\right] && \text{for } \phi_d-\pi \le \theta \le \phi_d \\ &\simeq -\frac{\epsilon^2 R}{8} && \text{for } \phi_d \le \theta \le \phi_d+\pi \end{aligned} \tag{4.24}$$

The evaluation of $\bar{r}_p(\theta)$ needs a few steps of computation.

$$\begin{aligned} 2\pi \bar{r}_p(\theta) &= \text{P.V.} \int_0^{2\pi} dt\, r_p(t)\cdot \cot\frac{t-\theta}{2} \\ &= \frac{a\epsilon^2}{2}\text{P.V.}\int_{\phi_d-\pi}^{\phi_d} dt \sin^2(t-\phi_d)\cdot \cot\frac{t-\theta}{2} \end{aligned} \tag{4.25}$$

By making the change of variables

$$t-\theta = x\,, \qquad \phi_d-\theta = y$$

and

$$\cot\frac{t-\theta}{2} = \frac{1+\cos x}{\sin x}\,,$$

the integrand of Eq. (4. 25) becomes

$$\sin^2(t-\phi_d)\cdot\cot\frac{t-\theta}{2} = \cos^2 y(\sin x+\frac{1}{2}\sin^2 x)$$

$$+\sin^2 y\cdot\frac{\cos^3 x+\cos^2 x}{\sin x} - \sin 2y(\cos x+\cos^2 x)\ . \qquad (4.26)$$

Substituting Eq. (4. 26) into Eq. (4. 25) and carrying out the integration, $\bar{r}_p(\theta)$ becomes

$$\bar{r}_p(\theta) = \frac{R\epsilon^2}{4\pi}\left[\sin^2(\theta-\phi_d)\cdot\mathrm{Log}\left\{\tan\frac{\theta-\phi_d}{2}\right\}^2 - 2\cos(\theta-\phi_d)+\frac{\pi}{2}\sin 2(\theta-\phi_d)\right]. \qquad (4.27)$$

This result will be applied in the next chapter to the problem of diffraction by a discontinuity in curvature.

CHAPTER V

FIELDS DIFFRACTED BY EDGES WITH DISCONTINUITIES IN CURVATURE

In this chapter fields diffracted by edges with discontinuities in curvature are obtained by asymptotically evaluating the contour integral derived in Section 4.1. First, in Section 5.1, various branch points are found. In Sections 5.2 and 5.3, the case when the edges are far from the shadow boundary, is considered. In Sections 5.4 and 5.5, the edges are taken to lie at the shadow boundaries. The summary of the results is tabulated in Section 5.6 and the physical meaning of these results is discussed in Chapter 6.

5.1 General Solution

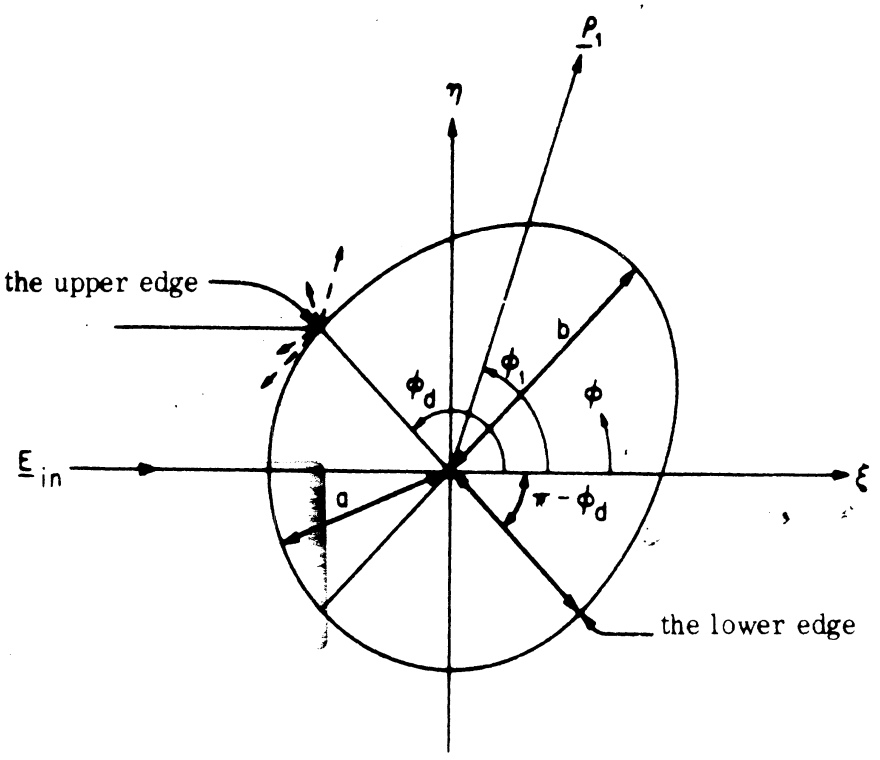

FIG. 5.1: THE SCATTERING BODY WITH TWO EDGES

Let the plane wave be incident on a perfectly conducting cylinder with two points of discontinuities in curvature as shown in Fig. 5.1 It is assumed that $\pi \geq \phi_1 \geq 0$ and $\pi \geq \phi_d \geq \frac{\pi}{2}$. At both junction points $\phi = \phi_d$ and $\phi = \phi_d - \pi$, curvatures of the semicircle and the semiellipse are $\frac{1}{a}$ and $\frac{1-\epsilon^2}{a}$ respectively, where ϵ is the eccentricity of the ellipse.

In order to apply the contour integral representation Eq. (4.14) of the edge effects, the boundary C_w in Fig. 5-1 is assumed to be almost circular (see Section 4.1).

The real part of the mapping function on the boundary is obtained in Section 4.2 and $g(\theta)$ is given as

$$g(\theta) = ik\left[\cos\theta \cdot r_p(\theta) - \sin\theta \cdot \bar{r}_p(\theta)\right] \tag{5.1}$$

where

$$\begin{aligned} r_p(\theta) &= \frac{\epsilon^2 R}{2}\left[\sin^2(\theta - \phi_d) - \frac{1}{4}\right] && \text{for } \phi_d - \pi \leq \theta \leq \phi_d \\ &= -\frac{\epsilon^2 R}{8} && \text{for } \phi_d \leq \theta \leq \phi_d + \pi \end{aligned} \tag{5.2}$$

and

$$\bar{r}_p(\theta) = \frac{\epsilon^2 R}{4\pi}\left[\sin^2(\theta - \phi_d) \cdot \mathrm{Log}\left(\tan\frac{\theta - \phi_d}{2}\right)^2 - 2\cos(\theta - \phi_d) + \frac{\pi}{2}\sin 2(\theta - \phi_d)\right].$$

$g(\theta)$ is a periodic function with the period 2π, and has branch points at $\theta = \phi_d$ and $\theta = \phi_d - \pi$. The branch point at $\theta = \phi_d$ is due to the discontinuity in curvature at $\theta = \phi_d$ on the surface of the scattering body, and the other branch point due to the discontinuity in curvature at $\theta = \phi_d - \pi$ (see Fig. 5-1).

Substituting Eq. (5.1) into (4.14), the fields diffracted by the two edges at the position of the circle-ellipse join are given by the following branch cut integrals

$$\tilde{u}_d(\rho_1) \cong \sqrt{\frac{2}{\pi k \rho_1}}\, e^{ik\rho_1 - i\frac{\pi}{4}} \left[\sigma + \sigma^*\right] \tag{5.3}$$

where

$$\sigma = -i\frac{M^2}{2} \int_{C_d} d\tilde{v}\, e^{-\tilde{v}}\, \frac{d\theta}{d\tilde{v}} \cdot g(-\theta + \phi_1 + \pi)\tilde{f}\left\{\zeta = M(\frac{\pi}{2} - \theta)\right\}, \tag{5.4}$$

$$\sigma^* = i\frac{M^2}{2} \int_{C_d^*} d\tilde{v}^*\, e^{-\tilde{v}^*}\, \frac{d\theta}{d\tilde{v}^*} \cdot g(-\theta + \phi_1 + \pi) \cdot \tilde{f}\left\{\zeta = M(\frac{\pi}{2} + \theta)\right\}, \tag{5.5}$$

and $g(\theta)$ is given by Eq. (5.1). The contours C_d and C_d^* are branch cut contours near the branch points of $g(\theta)$.

Various branch points of the integrand of σ in the range of integration can be easily found. First the saddle points are solutions of

$$\frac{d\tilde{v}}{d\theta} = -ikR\, \frac{d}{d\theta}\left[-\cos(\phi_1 - \theta) + \frac{\pi}{2} - \theta\right] = 0. \tag{5.6}$$

Solving Eq. (5.6) it can be shown that the saddle points lie at

$$\theta_{sn} = \phi_1 + \frac{\pi}{2} - 2n\pi \tag{5.7}$$

where $n = 0, 1, 2, \ldots,$.

The argument $\zeta = M(\frac{\pi}{2} - \theta)$ of the Fock function (see Eq. (4.6)) near these saddle points is positive except for the case $n=0$. When $n=0$, the argument

$\zeta = M(\frac{\pi}{2} - \theta_{so}) = -M\phi_1$ goes to negative infinity as $M \to \infty$ unless $\phi_1 = 0$. As discussed in Section 4.1, when the argument of the Fock function becomes a large negative value, the Fock function should be replaced by its asymptotic form. Unless $\phi_1 \simeq 0$, the new saddle point is a solution of

$$\frac{d\tilde{v}}{d\theta} = -ikR \frac{d}{d\theta}\left[\cos\theta - \cos(\phi_1 - \theta)\right] = 0. \tag{5.8}$$

The new saddle point is

$$\theta'_{so} = \frac{\phi_1}{2} + \frac{\pi}{2}.$$

Therefore, the saddle point lies at

$$\theta_{sn} = \phi_1 + \frac{\pi}{2} - 2n\pi \quad \text{where } n=1,2,\ldots,$$

and

$$\theta_{so} = \phi_1 + \frac{\pi}{2} \qquad \text{for } \phi_1 \simeq 0 \tag{5.9}$$

$$\theta'_{so} = \frac{\phi_1}{2} + \frac{\pi}{2} \qquad \text{for } \phi_1 > 0.$$

The branch points of $g(-\theta + \phi_1 + \pi)$ lie at

$$\theta_{dn} = \phi_1 - \phi_d + \pi - 2n\pi \quad \text{where } n=0,1,2\ldots, \tag{5.10}$$

due to the edge of the scattering body at $\phi=\phi_d$, and at

$$\bar{\theta}_{dn} = \theta_{dn} - \pi \tag{5.10'}$$

due to the edge at $\phi=\phi_d-\pi$. In the $\tilde{v}$ plane branch cuts are taken parallel to the real axis.

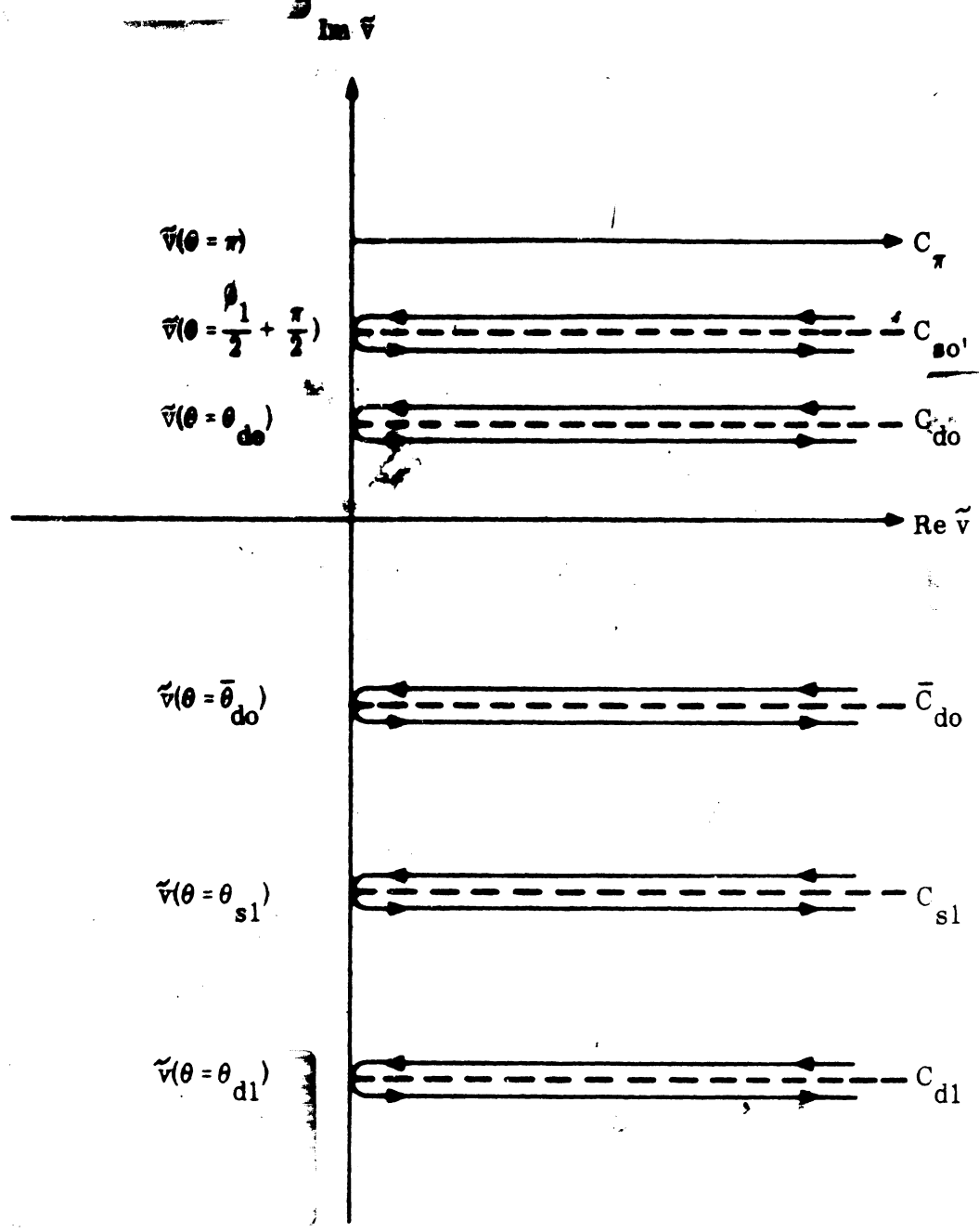

FIG. 5.2: $\tilde{\nu}$-PLANE

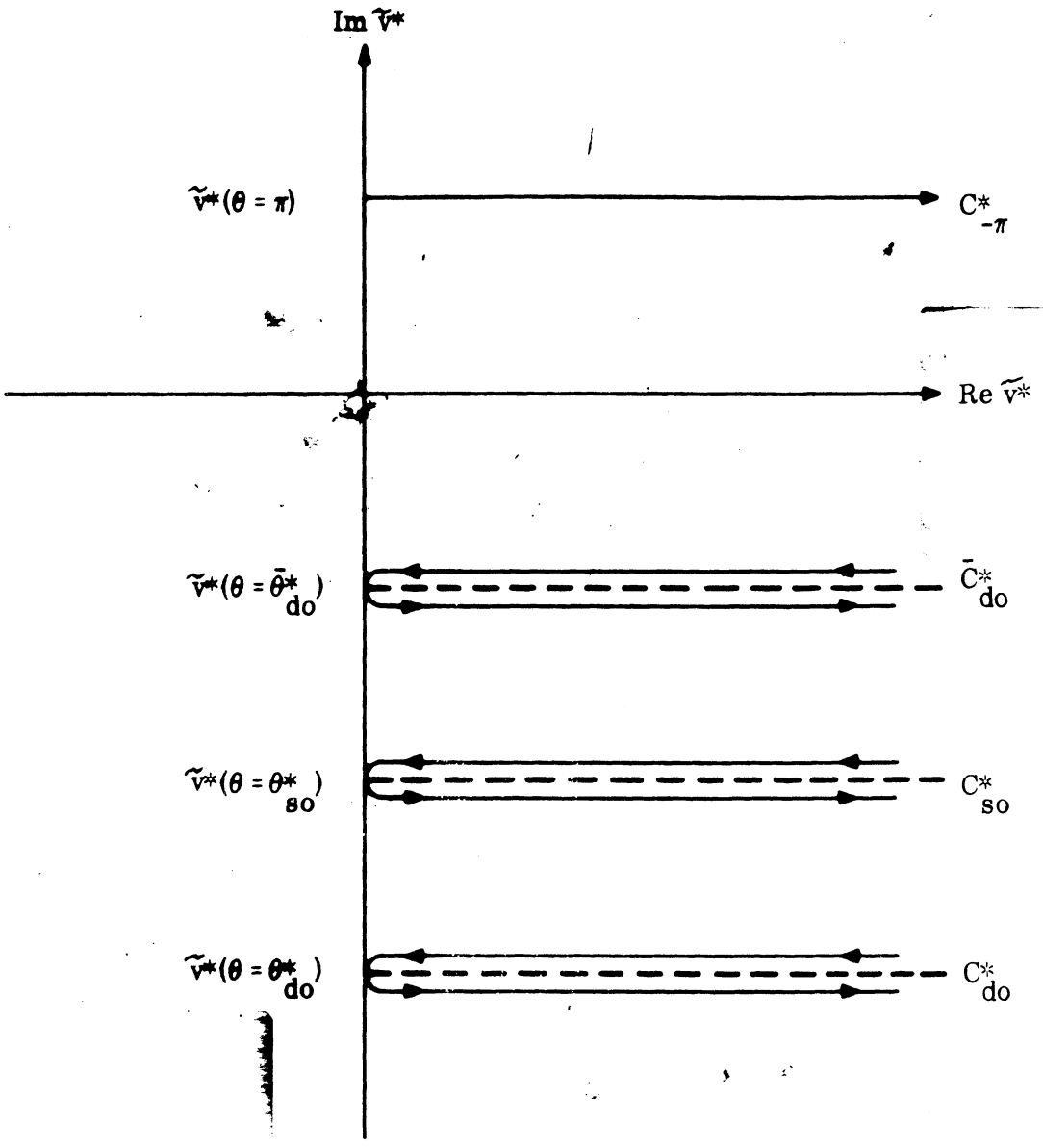

FIG. 5.3: $\tilde{v}^*$-PLANE

In a similar way, branch points for the integrand of σ^* can be obtained. Solving the following equation

$$\frac{d\tilde{v}^*}{d\theta} = -ikR \frac{d}{d\theta}\left[-\cos(\phi_1 - \theta) + \theta + \frac{\pi}{2}\right] = 0 , \qquad (5.11)$$

the saddle points lie at

$$\theta^*_{sn} = \phi_1 - \frac{\pi}{2} + 2n\pi \qquad \text{where} \quad n=0,1,2,\ldots \qquad (5.12)$$

Near all saddle points given by Eq. (5.12), the argument of the Fock function $\zeta = M(\frac{\pi}{2} + \theta^*_{sn})$ is positive $g(-\theta + \pi + \phi_1)$ in the integrand of σ^* has branch points at

$$\theta^*_{dn} = \phi_1 - \phi_d + \pi \pm 2n\pi \qquad \text{where} \quad n=0,1,2,\ldots \qquad (5.13)$$

due to the edge of the scattering body at $\phi=\phi_d$, and at

$$\bar{\theta}^*_{dn} = \theta^*_{dn} - \pi \qquad (5.14)$$

due to the edge at $\phi = \phi_d - \pi$.

In the $\tilde{v}^*$ plane branch cuts are taken parallel to the real axis.

The branch cut contours C_d and C^*_d which are introduced due to singularities of the mapping function are rewritten as

$$C_d = C_{do} + \bar{C}_{do} + C_{d1} + \ldots \qquad (5.15)$$

and

$$C^*_d = \overline{C^*_{do}} + C^*_{do} + \ldots , \qquad (5.16)$$

as long as any of these branch cuts of Eqs. (5.15) and (5.16) do not coincide with any branch cut due to the saddle point.

Since the branch points of the function $g(\theta)$ are dependent on ϕ_d (the position of the edge), while the saddle points are not, only the positions of the branch points of $g(\theta)$ are changed as the position of the edge is moved.

Let us evaluate each contour integral asymptotically for high frequency, in various cases, by changing the observation point $(\rho_1 e^{i\phi_1})$ and the position of the edge.

5.2 Case I. $\pi \geq \phi_1 > \phi_d - \frac{\pi}{2}$ and $\phi_d \neq \frac{\pi}{2}$

In this case the edge at $\phi = \phi_d$ is in the illuminated region and this edge can be directly seen from the observation point. Let us first assume that $\phi_1 \neq 2(\phi_d - \frac{\pi}{2})$, then none of the branch cuts due to the saddle points and singularities of the mapping function coincide in $\tilde{v}$ and $\tilde{v}^*$ planes.

(i) Evaluation of $\sigma(C_{do})$

Near the first branch point $\theta = \theta_{do} = \phi_1 - \phi_d + \pi$ in the $\tilde{v}$ plane, the argument of the Fock function $\zeta = M(-\frac{\pi}{2} + \theta_{do})$ is negative, so the function $e^{\pm ikR(\pi/2 - \theta)} \tilde{f}\{\zeta = M(\pi/2 - \theta)\}$ in the integrand of σ is replaced by its asymptotic form near this branch point. Near $\theta = \theta_{do}$

$$\tilde{v} = ikR\left[\cos(\phi_1 - \theta) - \cos\theta\right] \simeq i2kR \sin\frac{\phi_1}{2} \sin(\phi_d - \frac{\phi_1}{2}) - \tau \cdot i2kR \sin\frac{\phi_1}{2} \cos(\frac{\phi_1}{2} - \phi_d) \tag{5.17}$$

where

$$\tau = \theta - \theta_{do} .$$

Define

$$v = -i2kR \sin\frac{\phi_1}{2} \cdot \cos\left(\phi_d - \frac{\phi_1}{2}\right),$$

$$\tau_+ = \frac{e^{i\pi/2} v}{4M^3 \sin\frac{\phi_1}{2} \cdot \cos\left(\phi_d - \frac{\phi_1}{2}\right)} \qquad \text{for } \operatorname{Im} v > 0, \qquad (5.18)$$

and

$$\tau_- = \frac{e^{i\,5\pi/2} v}{4M^3 \sin\frac{\phi_1}{2} \cdot \cos\left(\phi_d - \frac{\phi_1}{2}\right)} \qquad \text{for } \operatorname{Im} v < 0.$$

Using Eq. (5.18), the branch cut contour integration of σ at $\theta = \theta_{do}$ becomes

$$\sigma(C_{do}) \simeq M^3 \cos(\phi_1 - \phi_d + \pi) \cdot \exp\left\{-i2kR \sin\frac{\phi_1}{2} \sin\left(\phi_d - \frac{\phi_1}{2}\right)\right\} I_{c_{do}} \qquad (5.19)$$

where

$$I_{c_{do}} = \int_0^\infty dv\, e^{-v}\left[\frac{d\tau_-}{dv} \cdot g(\phi_d - \tau_-) - \frac{d\tau_+}{dv} g(\phi_d - \tau_+)\right]. \qquad (5.20)$$

Near $v=0$, $\frac{d\tau}{dv}$ is analytic, but $g(\phi_d - \tau)$ is not and the second order term of the two sides of the branch cut are different (see Eq. (5.1) and Section 4.2).

Substituting Eq. (5.1) into Eq. (5.20), $I_{c_{do}}$ becomes

$$I_{c_{do}} \simeq \frac{i}{2M^3 \sin\frac{\phi_1}{2} \cdot \cos\left(\frac{\phi_1}{2} - \phi_d\right)} \int_0^\infty dv\, e^{-v}\left[g(\phi_d - \tau_-) - g(\phi_d - \tau_+)\right]$$

$$= \frac{2\epsilon^2(-\cos\phi_d + 2i\sin\phi_d)}{M^6\left[4\sin\frac{\phi_1}{2} \cdot \cos\left(\frac{\phi_1}{2} - \phi_d\right)\right]^3}. \qquad (5.21)$$

Since

$$\epsilon^2 \simeq R\left(\frac{1}{a} - \frac{1-\epsilon^2}{a}\right) \quad \text{(see Eq. (4.22) and (4.23))},$$

then

$$\frac{\epsilon^2}{M^3} = \frac{2\epsilon^2}{kR} \simeq \frac{2\left(\frac{1}{a} - \frac{1-\epsilon^2}{a}\right)}{k} \,. \tag{5.22}$$

Substituting Eq. (5.22) into Eq. (5.21), $\sigma(C_{do})$ becomes

$$\sigma(C_{do}) \simeq -\frac{\left(\frac{1}{a} - \frac{1-\epsilon^2}{a}\right)\left(-\cos\phi_d + 2i\sin\phi_d\right)\cdot\cos(\phi_1 - \phi_d)}{k\,16\left[\sin\frac{\phi_1}{2}\cdot\cos\left(\frac{\phi_1}{2} - \phi_d\right)\right]^3}\cdot \exp\left\{-i2kR\sin\frac{\phi_1}{2}\sin\left(\phi_d - \frac{\phi_1}{2}\right)\right\} \tag{5.23}$$

$\sigma(C_{do})$ is proportional to the difference of the two curvatures at the join $\phi=\phi_d$ and is of order $1/k$.

(ii) Evaluation of $\sigma(\bar{C}_{do})$

Near $\theta = \bar{\theta}_{do} = \phi_1 - \phi_d$, the argument of the Fock function $\zeta = M\left(\frac{\pi}{2} - \bar{\theta}_{do}\right)$ is positive, and

$$\begin{aligned} \tilde{v} &= ikR\left[\cos(\phi_1 - \theta) + \theta - \frac{\pi}{2}\right] \\ &\simeq ikR\left[-\cos\phi_d + \phi_1 - \phi_d - \frac{\pi}{2}\right] + ikR\left[1 + \sin\phi_d\right]\cdot\tau \end{aligned} \tag{5.24}$$

where

$$\tau = \theta - \bar{\theta}_{do} \,.$$

Set

$$v = ikR\left[1 + \sin\phi_d\right]\cdot\tau \,,$$

$$\tau_+ = \frac{e^{-i\frac{\pi}{2}} v}{\left[1+\sin\phi_d\right] 2M^3} \qquad \text{for } \mathrm{Im}\, v > 0$$

and

$$\tau_- = \frac{e^{-i\frac{5\pi}{2}} v}{\left[1+\sin\phi_d\right] 2M^3} \qquad \text{for } \mathrm{Im}\, v < 0 \ . \tag{5.25}$$

Using Eq. (5.24) and (5.25), the branch cut integral of σ at $\theta=\bar{\theta}_{do}$ becomes

$$\sigma(\bar{C}_{do}) \simeq -i\frac{M^2}{2}\tilde{f}\left\{\zeta=M(\frac{\pi}{2}+\phi_d-\phi_1)\right\} \cdot \exp\left\{ikR(\frac{\pi}{2}+\phi_d-\phi_1)\right.$$

$$\left. + ikR\cos(\phi_d-\pi)\right\} \cdot I_{\bar{C}_{do}} = M^2\sqrt{\pi}\sum_{s=1}^{\infty}\frac{\exp\left\{i(kR+Mt_s)(\frac{\pi}{2}+\phi_d-\phi_1)\right\}}{w_1'(t_s)}$$

$$\cdot I_{\bar{C}_{do}} \cdot e^{ikR\cos(\phi_d-\pi)} \tag{5.26}$$

where

$$I_{\bar{C}_{do}} = \int_o^\infty dv\, e^{-v}\left[\frac{d\tau_-}{dv}\, g(\phi_d-\pi-\tau_-) - \frac{d\tau_+}{dv}\, g(\phi_d-\pi-\tau_+)\right] . \tag{5.27}$$

In Eq. (5.26) the Fock function is expanded in terms of the residues at $w_1(t)=0$ (see Eq. (4.17)). Eq. (5.27) can be evaluated by the same method as used in Eq. (5.20).

$$I_{\bar{C}_{do}} \simeq -\frac{(\frac{1}{a}-\frac{1-\epsilon^2}{a})\left[-\cos\phi_d+2i\sin\phi_d\right]}{kM^3 2\left[1+\sin\phi_d\right]^3} \ . \tag{5.28}$$

Inserting Eq. (5.28) into Eq. (5.26) we obtain

$$\sigma(\bar{C}_{do}) \simeq \frac{\left(\frac{1}{a} - \frac{1-\epsilon^2}{a}\right)\left[\cos\phi_d - 2i\sin\phi_d\right]}{2k\left[1+\sin\phi_d\right]^3} \cdot \sqrt{\pi} \sum_{s=1}^{\infty} \frac{\exp\left\{i(kR+Mt_s)\left(\frac{\pi}{2}+\phi_d-\phi_1\right)\right\}}{M w_1'(t_s)}$$

$$\cdot \exp\left\{ikR\cos(\phi_d-\pi)\right\} . \qquad (5.29)$$

The phase term of Eq. (5.29) shows a new creeping wave contribution traveling in the clockwise direction, which appears to be due to diffracted fields of the incident plane wave $e^{ikR\cos(\phi_d-\pi)}$ by the edge at $\phi=\phi_d-\pi$, but this edge is in the shadow region. The only incident waves at the edge in the shadow region are creeping waves launched from the upper and the lower shadow boundaries. Therefore, the proper interpretation of the term $\exp\left\{ikR\cos(\phi_d-\pi)\right\}$ in Eq. (5.29) is necessary. Also we need the proper choice of either one or both of two incident creeping waves as the source. Suppose Eq. (5.29) represents diffracted fields of the incident creeping wave from the upper shadow boundary. Then the creeping waves, which are diffracted fields of the incident plane wave at the upper shadow boundary, and $\sigma(\bar{C}_{do})$ will have the same phase, and these two are indistinguishable (see Section 5.5). Furthermore, the creeping wave due to the diffraction at the shadow boundary is of order $k^{-1/3}$, and this term is dominant compared to that of Eq. (5.2) which is of order k^{-1}. So $\sigma(\bar{C}_{do})$ must represent the diffracted fields of the incident creeping wave from the lower shadow boundary (see Section 5.5).

Using the proper interpretation of the Fock function as a physical optics term or a creeping wave term (see Section 4.1), $\exp\left\{ikR\cos(\phi_d-\pi)\right\}$ term in

Eq. (5.29) is replaced by

$$\frac{\tilde{f}\left[\zeta=M\left(\frac{\pi}{2}+\phi_d-\pi\right)\right]}{2iM}\cdot\exp\left\{ikR\left(\frac{\pi}{2}+\phi_d-\pi\right)\right\}.$$

Therefore, $\sigma(\bar{C}_{do})$ becomes

$$\sigma(\bar{C}_{do})\simeq\frac{\left(\frac{1}{a}-\frac{1-\epsilon^2}{a}\right)(+\cos\phi_d-2i\sin\phi_d)}{2k\left[1+\sin\phi_d\right]^3}\cdot\sum_{s=1}^{\infty}\sum_{p=1}^{\infty}\frac{\pi\exp\left\{i(kR+Mt_s)\left(\frac{\pi}{2}+\phi_d-\phi_1\right)+i(kR+Mt_p)\left(\phi_d-\frac{\pi}{2}\right)\right\}}{M^2 w_1'(t_s)\,w_1'(t_p)} \tag{5.29)'}$$

(iii) Evaluation of $\sigma(C_{d1})$

Near $\theta=\theta_{d1}=\phi_1-\phi_d-\pi$, the argument of the Fock function $\zeta=M\left(\frac{\pi}{2}-\theta_{d1}\right)$ is positive, and

$$\tilde{v}=ikR\left[\cos(\phi_1-\theta)+\theta-\frac{\pi}{2}\right]$$

$$\simeq ikR\left[-\cos\phi_d+\phi_1-\phi_d-\frac{3}{2}\pi\right]+ikR\left[1-\sin\phi_d\right]\cdot\tau \tag{5.30}$$

where $\tau=\theta-\theta_{d1}$.

Define

$$v=i2M^3\left[1-\sin\phi_d\right]\cdot\tau,$$

$$\tau_+=\frac{e^{-i\pi/2}v}{2M^3\left[1-\sin\phi_d\right]}\qquad\text{for Im } v>0, \tag{5.31}$$

and

$$\tau_- = \frac{e^{-i\frac{5\pi}{2}} v}{2M^3\left[1-\sin\phi_d\right]} \qquad \text{for } \mathrm{Im}\, v<0 .$$

Substituting Eqs. (5.30) and (5.31) into Eq. (5.4), $\sigma(C_{d1})$ becomes

$$\sigma(C_{d1}) \simeq M^2\sqrt{\pi}\sum_{s=1}^{\infty}\frac{\exp\left\{i(kR+Mt_s)(-\phi_1+\phi_d+\frac{3}{2}\pi)+ikR\cos\phi_d\right\}}{w_1'(t_s)}$$

$$\cdot\int_0^{\infty} dv\, e^{-v}\left[\frac{d\tau_-}{dv}\,g(\phi_d-\tau_-) - \frac{d\tau_+}{dv}\,g(\phi_d-\tau_+)\right]$$

$$\simeq \frac{(\frac{1}{a}-\frac{1-\epsilon^2}{a})\left[-\cos\phi_d+2i\sin\phi_d\right]}{2k\left[1-\sin\phi_d\right]^3}$$

$$\cdot\sum_{s=1}^{\infty}\frac{\sqrt{\pi}\,\exp\left\{i(kR+Mt_s)(-\phi_1+\phi_d+\frac{3}{2}\pi)+ikR\cos\phi_d\right\}}{Mw_1'(t_s)} \qquad (5.32)$$

(iv) Evaluation of $\sigma^*(\bar{C}^*_{do})$

Near $\theta=\bar{\theta}^*_{do}=\phi_1-\phi_d$, the argument of the Fock function in σ^*, $\zeta=M(\frac{\pi}{2}+\bar{\theta}^*_{do})$ is positive, and

$$\tilde{v}^* = ikR\left[\cos(\phi_1-\theta)-\theta-\frac{\pi}{2}\right]$$

$$\simeq ikR\left[-\cos(\phi_d-\pi)-\phi_1+\phi_d-\frac{\pi}{2}\right] - ikR\left[1-\sin\phi_d\right]\cdot\tau \qquad (5.33)$$

Define

$$v = -ikR\left[1-\sin\phi_d\right]\tau ,$$

$$\tau_+ = \frac{e^{i5\pi/2}\, v}{2M^3\left[1-\sin\phi_d\right]} \qquad \text{for } \mathrm{Im}\, v>0 , \qquad (5.34)$$

and

$$\tau_- = \frac{e^{i\frac{\pi}{2}} v}{2\pi^3 \left[1-\sin\phi_d\right]} \qquad \text{for } \mathrm{Im}\, v < 0 \,. \tag{5.34}$$

Substituting Eqs. (5.33) and (5.34) into Eq. (5.5), the branch cut integral of σ^* at $\theta = \bar{\theta}^*_{do}$ becomes

$$\sigma^*(\bar{C}^*_{do}) \simeq \frac{(\frac{1}{a} - \frac{1-\epsilon^2}{a}) \left[\cos\phi_d - 2i\sin\phi_d\right]}{2k \left[1-\sin\phi_d\right]^3} \cdot e^{ikR\cos(\phi_d - \pi)}$$

$$\cdot \sum_{s=1}^{\infty} \frac{\sqrt{\pi}\ \exp\left\{i(kR + Mt_s)(\phi_1 - \phi_d + \frac{\pi}{2})\right\}}{M\, w_1'(t_s)} \tag{5.35}$$

Equation (5.35) represents fields diffracted by the edge in the shadow region. Therefore, by the same reason as the case of $\sigma(\bar{C}_{do})$ of Eq. (5.29), the plane wave term $\exp ikR\cos(\phi_d - \pi)$ in Eq. (5.35) is replaced by the creeping wave term $(2iM)^{-1} \cdot \tilde{f}\left\{M(\frac{\pi}{2} - \phi_d + \pi)\right\} \cdot \exp\left\{ikR(\frac{\pi}{2} - \phi_d + \pi)\right\}$. Substituting this factor into Eq. (5.35), we obtain diffracted fields of the incident creeping wave from the lower shadow boundary by the edge at $\phi = \phi_d - \pi$.

$$\sigma^*(\bar{C}^*_{do}) \simeq \frac{(\frac{1}{a} - \frac{1-\epsilon^2}{a}) \left[\cos\phi_d - 2i\sin\phi_d\right]}{2\pi \left[1-\sin\phi_d\right]^3}$$

$$\cdot \sum_{s=1}^{\infty} \sum_{p=1}^{\infty} \frac{\pi \exp\left\{i(kR + Mt_s)(\frac{\pi}{2} + \phi_1 - \phi_d) + i(kR + Mt_p)(\frac{3\pi}{2} - \phi_d)\right\}}{M^2 w_1'(t_s) w_1'(t_p)} \tag{5.35}'$$

(v) Evaluation of $\sigma^*(C^*_{do})$

Near $\theta=\theta^*_{do} = \phi_1-\phi_d+\pi$, the argument of the Fock function of σ^*, $\zeta=M(\frac{\pi}{2}+\theta^*_{do})$ is positive, and

$$\tilde{v}^* = ikR\left[\cos(\phi_1-\theta)-\theta-\frac{\pi}{2}\right]$$

$$\simeq ikR\left[-\phi_1+\phi_d-\frac{3}{2}\pi-\cos\phi_d\right] -ikR\left[1+\sin\phi_d\right]\cdot\tau \qquad (5.36)$$

where $\tau=\theta-\theta^*_{do}$.

Define

$$v=-ikR\left[1+\sin\phi_d\right]\tau,$$

$$\tau_+ = \frac{e^{i\frac{5\pi}{2}}\,v}{2M^3\left[1+\sin\phi_d\right]} \qquad \text{for } \mathrm{Im}\,v>0,$$

and

$$\tau_- = \frac{e^{i\frac{\pi}{2}}\,v}{2M^3\left[1+\sin\phi_d\right]} \qquad \text{for } \mathrm{Im}\,v<0. \qquad (5.37)$$

Substituting Eqs. (5.36) and (5.37) into Eq. (5.5), the branch cut integral of σ^* at $\theta=\theta^*_{do}$ becomes

$$\sigma^*(C^*_{do}) \simeq \frac{(\frac{1}{a}-\frac{1-\epsilon^2}{a})(\cos\phi_d-2i\sin\phi_d)}{2k\left[1+\sin\phi_d\right]^3}\cdot\sum_{s=1}^{\infty}\frac{\sqrt{\pi}\,\exp\left\{i(kR+Mt_s)(\frac{3}{2}\pi+\phi_1-\phi_d)+ikR\cos\phi_d\right\}}{M\,w_1'(t_s)}$$

(5.38)

When $\pi\geq\phi_1>\phi_d-\frac{\pi}{2}$, $\phi_d\neq\frac{\pi}{2}$ and $\phi_1\neq 2(\phi_d-\frac{\pi}{2})$, the fields diffracted by two edges are given as

$$\tilde{u}_d(\rho_1) \simeq \sqrt{\frac{2}{\pi k \rho_1}}\, e^{ik\rho_1 - i\frac{\pi}{4}} \Big[\sigma(C_{do}) \text{ of Eq. (5.23)} + \sigma(\bar{C}_{do}) \text{ of Eq. (5.29)}'$$
$$+ \sigma(C_{d1}) \text{ of Eq. (5.32)} + \sigma^*(\bar{C}^*_{do}) \text{ of Eq. (5.35)}'$$
$$+ \sigma^*(C^*_{do}) \text{ of Eq. (5.38)} + \ldots \Big] . \qquad (5.39)$$

When $\phi_1 \simeq 2(\phi_d - \frac{\pi}{2})$, in $\tilde{v}$-plane of Fig. 5-2 two branch cuts at the saddle point $\theta=\theta'_{so} = \frac{\phi_1}{2} + \frac{\pi}{2}$ and the branch point of the mapping function $\theta=\theta_{do}=\phi_1-\phi_d+\pi$ coincide. In Eq. (5.20) $\frac{d\tau}{dv}$ is not analytic any more near $\theta=\theta_{do}$, and $g(\phi_d-\tau_-)$ differs from $g(\phi_d-\tau_+)$ still in the second order term. Therefore, the saddle point contribution is dominant, and $\sigma(C_{do})$ of Eq. (5.23) disappears (see Appendix B). The other terms in Eq. (5.39) remain unchanged. Physically this means that when the specular reflection point and the position of the edge coincide, the specularly reflected field and the field diffracted by the edge are indistinguishable. The specularly reflected field remains unchanged in the first order approximation for high frequency.

5.3 Case II. $\phi_d - \frac{\pi}{2} > \phi_1 \geq 0$ and $\phi_d \neq \frac{\pi}{2}$

As the observation point moves across the tangent line at the position of the circle-ellipse join, the argument of $\tilde{f}\left\{M(\frac{\pi}{2}-\theta)\right\}$ near $\theta=\theta_{do}=\phi_1-\phi_d+\pi$ changes from a negative value to a positive value, and the argument of $\tilde{f}\left\{M(\frac{\pi}{2}+\theta)\right\}$ near $\theta=\theta^*_{do}=\phi_1-\phi_d$ changes from a positive value to a negative value. The relative position of the branch points due to the mapping function with respect to those due to the saddle points remain unchanged as in Case I.

(i) Evaluation of $\sigma(C_{do})$

Near $\theta=\theta_{do}=\phi_1-\phi_d+\pi$, the argument of the Fock function, $\xi=M(\frac{\pi}{2}-\theta_{do})$ is positive or equal to zero and in the integrand of σ of Eq. (5.4)

$$\tilde{v} = ikR\left[\cos(\phi_1-\theta)+\theta-\frac{\pi}{2}\right]$$
$$\simeq ikR\left[\phi_1-\phi_d+\frac{\pi}{2}-\cos\phi_d\right]+ikR\left[1-\sin\phi_d\right]\cdot\tau \qquad (5.40)$$

where $\tau=\theta-\theta_{do}$ (note the difference between Eq. (5.40) and Eq. (5.17)).

Define

$$v = ikR\left[1-\sin\phi_d\right]\tau ,$$

$$\tau_+ = \frac{e^{-i\frac{\pi}{2}}\, v}{2M^3\left[1-\sin\phi_d\right]} \qquad \text{for } \mathrm{Im}\, v > 0 , \qquad (5.41)$$

and

$$\tau_- = \frac{e^{-i\frac{5\pi}{2}}\, v}{2M^3\left[1-\sin\phi_d\right]} \qquad \text{for } \mathrm{Im}\, v < 0 .$$

Substituting Eqs. (5.40) and (5.41) into Eq. (5.4), the branch cut integral of σ at $\theta=\theta_{do}$ becomes

$$\sigma(C_{do}) \simeq \frac{(\frac{1}{a}-\frac{1-\epsilon^2}{a})(-\cos\phi_d+2i\sin\phi_d)}{k^2\left[1-\sin\phi_d\right]^3}\sum_{s=1}^{\infty}\frac{\sqrt{\pi}\exp\left\{i(kR+Mt_s)(\phi_d-\frac{\pi}{2}-\phi_1)+ikR\cos\phi_d\right\}}{M\, w_1'(t_s)} \qquad (5.42)$$

(ii) Evaluation of $\sigma^*(\bar{C}^*_{do})$

Near $\theta=\bar{\theta}^*_{do}=\phi_1-\phi_d$, the argument of the Fock function, $\xi=M(\frac{\pi}{2}+\theta)$, is almost equal to zero when $\phi_1 \simeq \phi_d-\frac{\pi}{2}$, and is negative when $\phi_1 < \phi_d-\frac{\pi}{2}$.

Therefore, when $\phi_1 < \phi_d - \frac{\pi}{2}$, the residue series of the Fock function in Eq. (5.35)' should be replaced by the asymptotic form of the Fock function for the negative argument,

$$\sigma^*(\bar{C}^*_{do}) \simeq \frac{(\frac{1}{a} - \frac{1-\epsilon^2}{a}) \left[\cos\phi_d - 2i\sin\phi_d\right] \sin(\phi_1 - \phi_d - \pi)}{2k \left[1 - \sin\phi_d\right]^3} \cdot \sum_{p=1}^{\infty} \frac{\sqrt{\pi}\, \exp\left\{i(kR + Mt_p)(\frac{3\pi}{2} - \phi_d) + ikR\sin(\phi_1 - \phi_d - \pi)\right\}}{M\, w_1'(t_p)} \quad (5.43)$$

$$\text{for } \phi_1 < \phi_d - \frac{\pi}{2} .$$

$\sigma(\bar{C}_{do})$, $\sigma(C_{d1})$ and $\sigma^*(C^*_{do})$ are the same as those given in the previous section, and the fields diffracted by two edges are

$$\tilde{u}_d(\rho_1) \simeq \sqrt{\frac{2}{\pi k \rho_1}}\, e^{ik\rho_1 - i\frac{\pi}{4}} \Big[\sigma(C_{do}) \text{ of Eq. (5.42)} + \sigma(\bar{C}_{do}) \text{ of Eq. (5.29)'} + \sigma(C_{d1}) \text{ of Eq. (5.32)} + \sigma^*(\bar{C}^*_{do}) \text{(see the next paragraph)} + \sigma^*(C^*_{do}) \text{ of Eq. (5.38)} + \ldots\Big] \quad \text{for } \phi_d - \frac{\pi}{2} \gtrsim \phi_1 > 0 \text{ and } \phi_d > \frac{\pi}{2} . \quad (5.44)$$

In Eq. (5.44) $\sigma^*(\bar{C}^*_{do})$ is given by Eq. (5.35)', when $\phi_1 \simeq \phi_d - \frac{\pi}{2}$, and by Eq. (5.43) when $\phi_1 < \phi_d - \frac{\pi}{2}$.

5.4 Case III. $\pi > \phi_1 > 0$ and $\phi_d = \frac{\pi}{2}$.

When ϕ_d becomes $\frac{\pi}{2}$, the position of the circle-ellipse join lies at the shadow boundary, and the relative positions of the branch points of the mapping function with respect to those due to the saddle points are changed in Fig. 5-2 and

Fig. 5-3. In fact, $\theta_{d1}=\phi_1-\frac{3}{2}\pi$ (Eq. (5.10)) becomes equal to θ_{s1} (Eq. (5.9)), and $\bar{\theta}^*_{do}=\phi_1-\frac{\pi}{2}$ (Eq. (5.14)) becomes equal to θ^*_{s1} (Eq. (5.12)). Thus, two branch cuts at $\theta=\theta_{d1}$ and $\theta=\theta_{s1}$ in Fig. 5-2 coincide, and two branch cuts at $\theta=\bar{\theta}^*_{do}$ and $\theta=\theta^*_{so}$ in Fig. 5-3 coincide.

(i) Evaluation of $\sigma(C_{do})$

$\sigma(C_{do})$ is the same as that of Eq. (5.23), and substituting $\phi_d=\frac{\pi}{2}$ into Eq. (5.23), $\sigma(C_{do})$ becomes

$$\sigma(C_{do}) \simeq -\frac{(\frac{1}{a}-\frac{1-\epsilon^2}{a})\sin\phi_1}{k\left[1-\cos\phi_1\right]^3}\exp\left\{-ikR\sin\phi_1+i\frac{\pi}{2}\right\}. \qquad (5.45)$$

(ii) Evaluation of $\sigma(\bar{C}_{do})$

In Case I of Section 5.2, the position of the circle-ellipse join at $\phi=\phi_d-\pi$ was in the shadow region and therefore was unable to be directly reached by the incident plane wave. But in the case of $\phi_d=\frac{\pi}{2}$, this edge lies at the shadow boundary. So Eq. (5.29) is valid, and substituting $\phi_d=\frac{\pi}{2}$ into Eq. (5.28), $\sigma(\bar{C}_{do})$ is obtained.

$$\sigma(\bar{C}_{do}) \simeq \frac{(\frac{1}{a}-\frac{1-\epsilon^2}{a})}{k\beta}\sum_{s=1}^{\infty}\frac{\sqrt{\pi}\exp\left\{i(kR+Mt_s)(\pi-\phi_1)-i\frac{\pi}{2}\right\}}{M\,w_1'(t_s)} \qquad (5.46)$$

(iii) Evaluation of $\sigma(C_{d1})$ and $\sigma^*(\bar{C}^*_{do})$

Both branch cuts at $\theta=\theta_{d1}$ in Fig. 5-2 and at $\theta=\bar{\theta}^*_{do}$ in Fig. 5-3 coincide with branch cuts due to saddle points. $\sigma(C_{d1})$ and $\sigma^*(\bar{C}^*_{do})$ are indistinguishable from contour integrals of saddle points (see Appendix B).

(iv) Evaluation of $\sigma^*(C^*_{do})$

$\sigma^*(C^*_{do})$ remains the same as Eq. (5.38) of Case I, and substituting $\phi_d = \frac{\pi}{2}$ in Eq. (5.38), $\sigma^*(C^*_{do})$ becomes

$$\sigma^*(C^*_{do}) \simeq \frac{(\frac{1}{a} - \frac{1-\epsilon^2}{a})}{k8} \sum_{s=1}^{\infty} \frac{\sqrt{\pi}\, \exp\left\{i(kR+Mt_s)(\pi+\phi_1)+i\frac{\pi}{2}\right\}}{M w_1'(t_s)} \quad . \qquad (5.47)$$

So when $\pi > \phi_1 > 0$ and $\phi_d = \frac{\pi}{2}$, the edge-effects are:

$$\tilde{u}_d(\rho_1) \simeq \sqrt{\frac{2}{\pi k \rho_1}}\, e^{ik\rho_1 - i\frac{\pi}{4}} \left[\sigma(C_{do}) \text{ of Eq. (5.45)} + \sigma(\bar{C}_{do}) \text{ of Eq. (5.46)} + \sigma^*(C^*_{do}) \text{ of Eq. (5.47)} + \ldots\right] . \qquad (5.48)$$

5.5 Case IV-A $\phi_1 \simeq \pi$ and $\phi_d = \frac{\pi}{2}$, and Case IV-B $\phi_1 \simeq 0$ and $\phi_d = \frac{\pi}{2}$

(i) Case IV-A: $\phi_1 \simeq \pi$ and $\phi_d = \frac{\pi}{2}$

Near $\theta = \theta_{do} = \phi_1 - \phi_d + \pi$, the argument of the Fock function, $\zeta = M(\frac{\pi}{2} - \theta)$ is almost equal to zero. Near $\phi_1 \simeq \pi$

$$-kR \sin\phi_1 = kR(\phi_1 - \pi) + \frac{M^3}{3}(\phi_1 - \pi)^3 . \qquad (5.49)$$

Using the relationship of Eq. (5.49), the physical optics term $\sin\phi_1 e^{-ikR\sin\phi_1}$ in Eq. (5.45) is replaced by the Fock function

$$-(i2M)^{-1} \exp\left\{ikR(\phi_1 - \pi)\right\} \cdot \tilde{f}\left[\zeta = M(\phi_1 - \pi)\right]$$

$$\sigma(C_{do}) \simeq \frac{(\frac{1}{a} - \frac{1-\epsilon^2}{a})}{k16\sqrt{\pi}\, M} \tilde{f}\left[\zeta = M(\phi_1 - \pi)\right] \cdot \exp\left\{ikR(\phi_1 - \pi)\right\} \qquad (5.50)$$

When $\phi_1 \simeq \pi$ and $\phi_d = \frac{\pi}{2}$, the edge-effects are the same as Eq. (5.48) except $\sigma(C_{do})$ which is given by Eq. (5.50) instead of Eq. (5.45).

(ii) Case IV-B: $\phi_1 \simeq 0$ and $\phi_d = \frac{\pi}{2}$

When $\phi_1 \simeq 0$ the observation point is near or in the shadow region, and the saddle point lies at $\theta = \theta_{so} = \frac{\pi}{2} + \phi_1$ instead of $\theta'_{so} = \frac{\pi}{2} + \frac{\phi_1}{2}$ (see Eq. (5.9)). So in Fig. 5-2, the two branch cuts at $v(\theta = \theta_{so})$ and at $v(\theta = \theta_{do} = \phi_1 - \phi_d + \pi)$ coincide, and $\sigma(C_{do})$ is indistinguishable from the saddle point contribution (see Appendix B).

Physically, this means that as the observation point approaches the shadow region, the specularly reflected field disappears and a diffracted field at the shadow boundary appears, and this field is indistinguishable from the field diffracted by the edge in the forward direction. Therefore, when $\phi_1 \simeq 0$ and $\phi_d = \frac{\pi}{2}$, the edge-effects are the same as those of Eq. (5.48) except $\sigma(C_{do})$ which disappears.

5.6 Summary of the Results

In this section, various expressions of the diffracted fields obtained in this chapter are tabulated for convenience.

The scattering body investigated is constructed by smoothly joining a semi-circle of radius a and a semi-ellipse of minor axis 2a and eccentricity ϵ. At the two positions of the circle-ellipse join ($\phi = \phi_d$ and $\phi = \phi_d - \pi$), curvatures of the circle and the ellipse are $\frac{1}{a}$ and $\frac{1-\epsilon^2}{a}$ respectively (see Fig. 5-4).

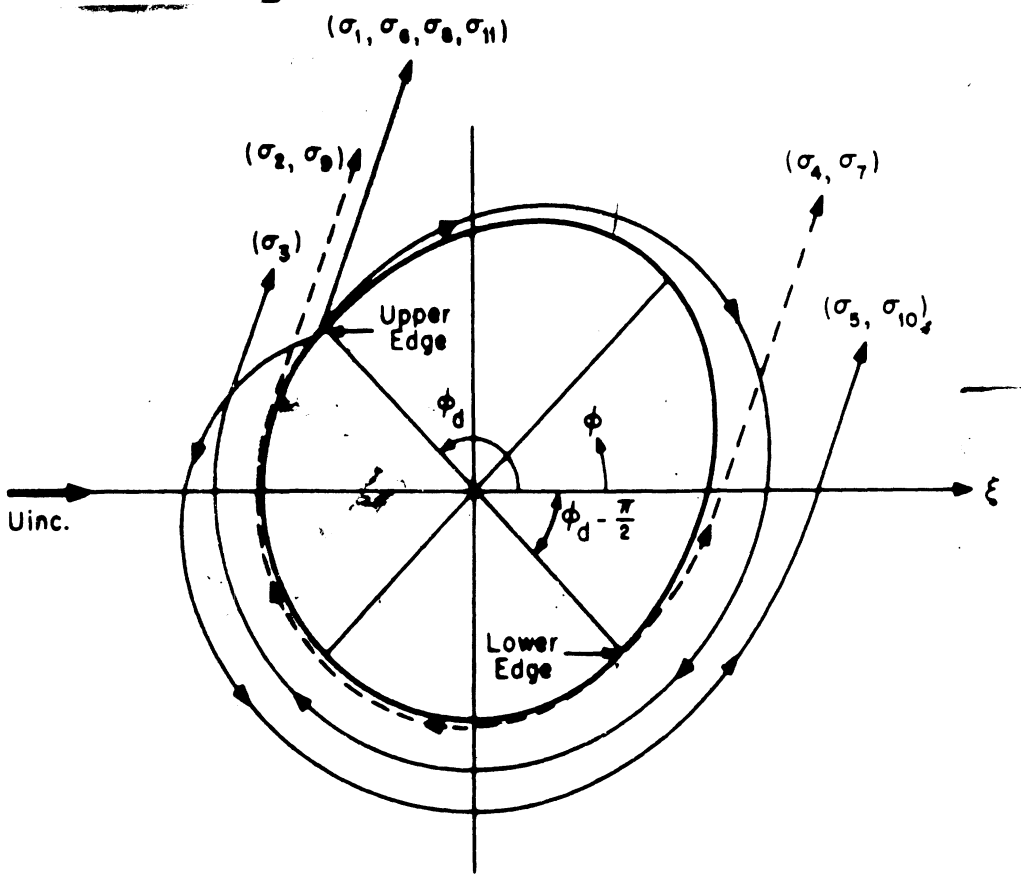

$\longrightarrow$ ray diffracted by the upper edge

$\dashrightarrow$ ray diffracted by the lower edge

FIG. 5. 4: VARIOUS RAYS DIFFRACTED BY EDGES

For simplicity, the fields diffracted by both edges with discontinuities in curvature are denoted as

$$\tilde{u}_d(\rho_1) = \sqrt{\frac{2}{\pi k \rho_1}}\, e^{ik\rho_1 - i\frac{\pi}{4}}\, \sigma \qquad (5.51)$$

where $\rho_1 = \rho_1 e^{i\phi_1}$ is the observation point. σ is given in the following Table V-1 for various cases.

TABLE 5-1: AMPLITUDES OF FIELDS DIFFRACTED BY EDGES

Case No.	ϕ_d	ϕ_1	σ	Reference
I	$\phi_d > \frac{\pi}{2}$	$\pi \geq \phi_1 > \phi_d - \frac{\pi}{2}$ $\phi_1 \neq 2(\phi_d - \frac{\pi}{2})$	$\sigma_1+\sigma_2+\sigma_3+\sigma_4+\sigma_5$	Eq. (5.39)
		$\phi_1 = 2(\phi_d - \frac{\pi}{2})$	$\sigma_2+\sigma_3+\sigma_4+\sigma_5$	Eq. (5.39)
II	$\phi_d > \frac{\pi}{2}$	$\phi_d - \frac{\pi}{2} > \phi_1 \geq 0$	$\sigma_6+\sigma_2+\sigma_3+\sigma_7+\sigma_5$	Eq. (5.44)
		$\phi_1 \simeq \phi_d - \frac{\pi}{2}$	$\sigma_6+\sigma_2+\sigma_3+\sigma_4+\sigma_5$	Eq. (5.44)
III	$\phi_d = \frac{\pi}{2}$	$\pi > \phi_1 > 0$	$\sigma_8+\sigma_9+\sigma'_{10}$	Eq. (5.48)
IV-A	$\phi_d = \frac{\pi}{2}$	$\phi_1 \simeq \pi$	$\sigma_{11}+\sigma_9+\sigma_{10}$	Section 5.5
IV-B	$\phi_d = \frac{\pi}{2}$	$\phi_1 \simeq 0$	$\sigma_9+\sigma_{10}$	Section 5.5

where

$$\sigma_1 = \frac{\left(\frac{1}{a} - \frac{1-\epsilon^2}{a}\right)(\cos\phi_d - 2i\sin\phi_d)\cos(\phi_1 - \phi_d)}{k2\left[\sin(\phi_1 - \phi_d) + \sin\phi_d\right]^3} \exp\left\{-i2kR\sin\frac{\phi_1}{2}\sin\left(\phi_d - \frac{\phi_1}{2}\right)\right\}$$

(see Eq. (5.23))

$$\sigma_2 = \frac{\left(\frac{1}{a} - \frac{1-\epsilon^2}{a}\right)(\cos\phi_d - 2i\sin\phi_d)\pi}{k2(1+\sin\phi_d)^3}$$

$$\cdot \sum_{s=1}^{\infty}\sum_{p=1}^{\infty} \frac{\exp\left\{i(kR+Mt_s)(-\phi_1+\phi_d+\frac{\pi}{2}) + i(kR+Mt_p)(\phi_d-\frac{\pi}{2})\right\}}{M^2 w_1'(t_s)\, w_1'(t_p)}$$

(see Eq. (5.29)')

$$\sigma_3 = \frac{\left(\frac{1}{a} - \frac{1-\epsilon^2}{a}\right)(-\cos\phi_d + 2i\sin\phi_d)\sqrt{\pi}}{k2(1-\sin\phi_d)^3}$$

$$\cdot \sum_{s=1}^{\infty} \frac{\exp\left\{i(kR+Mt_s)(-\phi_1+\phi_d+\frac{3}{2}\pi) + ikR\cos\phi_d\right\}}{M\, w_1'(t_s)}$$

(see Eq. (5.32))

$$\sigma_4 = \frac{\left(\frac{1}{a} - \frac{1-\epsilon^2}{a}\right)(\cos\phi_d - 2i\sin\phi_d)\pi}{k2\left\{1-\sin\phi_d\right\}^3}$$

$$\cdot \sum_{s=1}^{\infty}\sum_{p=1}^{\infty} \frac{\exp\left\{i(kR+Mt_s)(\phi_1-\phi_d+\frac{\pi}{2}) + i(kR+Mt_p)(\frac{3}{2}\pi-\phi_d)\right\}}{M^2 w_1'(t_s) w_1'(t_p)}$$

(see Eq. (5.35)')

$$\sigma_5 = \frac{\left(\frac{1}{a} - \frac{1-\epsilon^2}{a}\right)(\cos\phi_d - 2i\sin\phi_d)\sqrt{\pi}}{k2(1+\sin\phi_d)^3}$$

$$\cdot \sum_{s=1}^{\infty} \frac{\exp\left\{i(kR+Mt_s)(\phi_1-\phi_d+\frac{3}{2}\pi) + ikR\cos\phi_d\right\}}{M\, w_1'(t_s)}$$

(see Eq. (5.38))

$$\sigma_6 = \frac{\left(\frac{1}{a} - \frac{1-\epsilon^2}{a}\right)\left(\cos\phi_d + 2i\sin\phi_d\right)\sqrt{\pi}}{k2(1-\sin\phi_d)^3} \cdot \sum_{s=1}^{\infty} \frac{\exp\left\{i(kR+Mt_s)(-\phi_1+\phi_d-\frac{\pi}{2}) + ikR\cos\phi_d\right\}}{M\,w_1'(t_s)}$$

(see Eq. (5.42))

$$\sigma_7 = \frac{\sqrt{\pi}\left(\frac{1}{a} - \frac{1-\epsilon^2}{a}\right)\left(-\cos\phi_d + 2i\sin\phi_d\right)\sin(\phi_1-\phi_d)}{k2(1-\sin\phi_d)^3} \cdot \sum_{p=1}^{\infty} \frac{\exp\left\{-ikR\sin(\phi_1-\phi_d) + i(kR+Mt_p)(\frac{3}{2}\pi-\phi_d)\right\}}{M\,w_1'(t_p)}$$

(see Eq. (5.43))

$$\sigma_8 = -\frac{\left(\frac{1}{a} - \frac{1-\epsilon^2}{a}\right)i\sin\phi_1}{k\,(1-\cos\phi_1)} \exp\left\{-ikR\sin\phi_1\right\}$$

(see Eq. (5.45))

$$\sigma_9 = -\frac{\left(\frac{1}{a} - \frac{1-\epsilon^2}{a}\right)i\sqrt{\pi}}{k8} \sum_{s=1}^{\infty} \frac{\exp\left\{i(kR+Mt_s)(-\phi_1+\pi)\right\}}{M\,w_1'(t_s)}$$

(see Eq. (5.46))

$$\sigma_{10} = \frac{\left(\frac{1}{a} - \frac{1-\epsilon^2}{a}\right)i\sqrt{\pi}}{k8} \sum_{s=1}^{\infty} \frac{\exp\left\{i(kR+Mt_s)(\phi_1+\pi)\right\}}{M\,w_1'(t_s)}$$

(see Eq. (5.47))

$$\sigma_{11} = \frac{\left(\frac{1}{a} - \frac{1-\epsilon^2}{a}\right)}{k16\,\pi\,M} \int \left\{\zeta = M(\phi_1-\pi)\right\} \cdot \exp\left\{ikR(\phi_1-\pi)\right\},$$

(see Eq. (5.50))

CHAPTER VI

DISCUSSION

In this chapter, the physical meaning of the results obtained in Chapter 5 and the limitation of validity of these results are discussed, as well as the possibility of extending the present method to the case of Neumann boundary condition and diffraction by a wedge. It is difficult to give the precise amplitudes of the diffracted fields for an arbitrary jump in the curvature, so some of the remarks are conjectural.

Let us first discuss the diffracted fields in the case when the point of discontinuity in curvature lies in the illuminated region.

From Case I in the Table 5-1 of Section 5.6, it is shown that diffracted fields arrive at the observation point $\underline{\rho}_1$ both as a direct ray and as creeping waves launched in both tangential directions at the edge and circling around the scattering body (see Fig. 5-4).

The contribution of the direct ray from the discontinuity is given by σ_1 of Section 5.6 (or Eq. (5.23)).

$$\tilde{u}_d(\underline{\rho}_1) \simeq \sqrt{\frac{2}{\pi k \rho_1}}\, e^{ik\rho_1 - i\frac{\pi}{4}} \cdot \frac{\left(\frac{1}{R_1} - \frac{1}{R_2}\right)(\cos\phi_d - 2i\sin\phi_d)\cdot\cos(\phi_1 - \phi_d)}{2k\left[\sin(\phi_1 - \phi_d) + \sin\phi_d\right]^3} \tag{6.1}$$

(Note that the point of discontinuity is taken as the origin, and $\frac{1}{a}$ and $\frac{1-\epsilon^2}{a}$ are replaced by $\frac{1}{R_1}$ and $\frac{1}{R_2}$, respectively.)

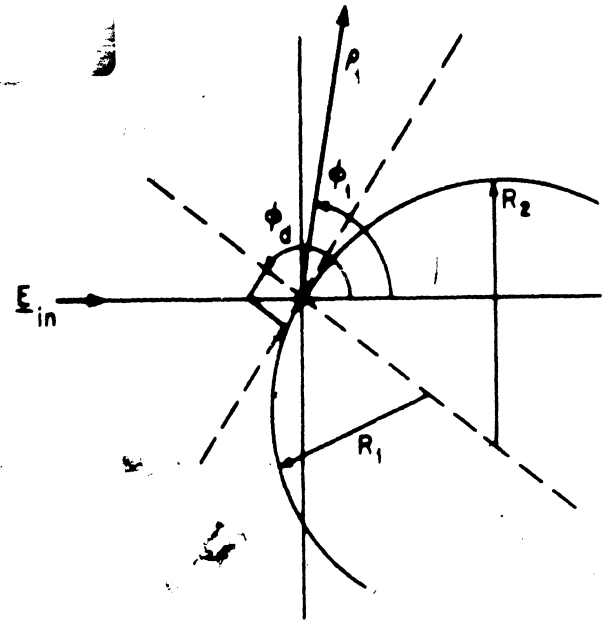

FIG. 6.1: DIRECT RAY FROM THE DISCONTINUITY

Eq. (6.1) is similar to that obtained by Weston[16] for the case of the Neumann boundary condition. The difference is that in Weston's result the numerator is given as $2+\cos(\phi_1-2\phi_d)-\cos\phi_1$ instead of the term $(\cos\phi_d-2i\sin\phi_d)\cos(\phi_1-\phi_d)$ in Eq. (6.1).

When the observation point moves across the tangential line such that $\phi_1 < \phi_d - \frac{\pi}{2}$, Case II in Table V-1 of Section 5.6 shows that the rays diffracted by the discontinuity reach the observation point as creeping waves, which are given by σ_6 of Section 5.6 as

$$u_d(\underline{\rho}_1) \simeq \sqrt{\frac{2}{\pi k \rho_1}}\, e^{ik\rho_1 - i\frac{\pi}{4}} \cdot \frac{\left(\frac{1}{R_1} - \frac{1}{R_2}\right)\left(-\cos\phi_d + 2i\sin\phi_d\right)}{2k(1-\sin\phi_d)^3}$$

$$\sum_{s=1}^{\infty} \frac{\sqrt{\pi}\exp\left\{i\left(kR + \left(\frac{kR}{2}\right)^{1/3} t_s\right)(\phi_d - \phi_1 - \frac{\pi}{2})\right\}}{\left(\frac{kR}{2}\right)^{1/3} w_1'(t_s)} \qquad (6.2)$$

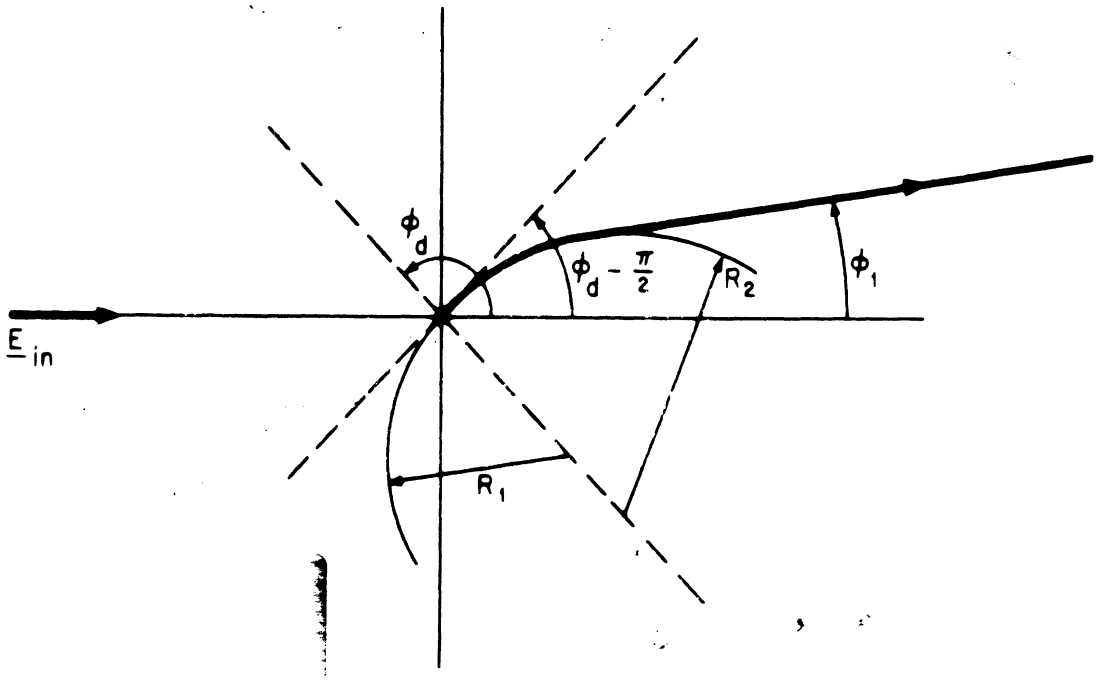

FIG. 6.2: THE CREEPING WAVE LAUNCHED BY THE DISCONTINUITY

In Eq. (6.2) R is the radius of curvature of the transformed circular boundary and is given as

$$R = a(1 + \frac{\epsilon^2}{8}) \qquad \text{by Eq. (4.23)} .$$

Suppose that we transform the given boundary of the scattering body into another contour (instead of a circle) such that a little away from the discontinuity, the transformed boundary is identical to the original boundary. Then the radius R in the second bracket of Eq. (6.2) would have become R_2.

Actually, this creeping wave launched by the discontinuity is propagating along the boundary whose curvature is $\frac{1}{R_2}$. Therefore, we may conjecture that the diffraction factor in the second bracket of Eq. (6.2) is modified by higher order iterated terms of the solution of the integral equation. (Note that it was shown in Section 2.3 that the iterated terms represent the effects of $\left|\frac{dw}{dz}\right|$ on the propagation of the radiated and the scattered fields. Also see Weston's works[15],[16].

With this consideration in mind $R=R_2$ is substituted in Eq. (6.2).

$$u_d(\rho_1) \simeq \sqrt{\frac{2}{\pi k \rho_1}}\, e^{ik\rho_1 - i\frac{\pi}{4}}\, \frac{(\frac{1}{R_1} - \frac{1}{R_2})(-\cos\phi_d + 2i\sin\phi_d)}{2k(1-\sin\phi_d)^3}$$

$$\cdot \sum_{s=1}^{\infty} \frac{\sqrt{\pi}\, \exp\left\{i(kR_2 + (\frac{kR_2}{2})^{1/3})(\phi_d - \frac{\pi}{2} - \phi_1)\right\}}{(\frac{kR_2}{2})^{1/3}\, w_1'(t_s)} \qquad (6.2)'$$

When $\phi_1 \simeq 2\phi_d - \pi$, the specular reflection point and the point of discontinuity in curvature coincide, and the specularly reflected field and the field diffracted by the discontinuity become indistinguishable. The study in Section 5.2 and Appendix B

shows that in such a case the field diffracted by the discontinuity disappears, in first approximation for high frequency. Therefore, we may conjecture that when $\phi_1 \simeq 2\phi_d - \pi$ the specularly reflected field can still be obtained by the method of physical optics.

Next let us consider the case in which the point of discontinuity in curvature lies at the shadow boundary. Then the incident wave impinges tangentially on the curved boundary with a discontinuity in curvature (see Fig. 6-3). Again there are contributions of a direct ray and the creeping waves launched at the point of discontinuity in curvature.

When $\pi > \phi_1 > 0$ and $\phi_d = \frac{\pi}{2}$, the dominant term of the edge-effects is the direct ray which is given by Eq. (6.1). Substituting $\phi_d = \frac{\pi}{2}$ in Eq. (6.1) $\tilde{u}_d$ becomes

$$\tilde{u}_d(\rho_1) \simeq \sqrt{\frac{2}{\pi k \rho_1}}\, e^{ik\rho_1 - i\frac{3\pi}{4}} \cdot \frac{\left(\frac{1}{R_1} - \frac{1}{R_2}\right)\sin\phi_1}{k\left\{1-\cos\phi_1\right\}^3}. \tag{6.3}$$

When ϕ_1 is greater than π, the diffracted ray reaches the observation point only as a creeping wave, and with the same argument as that of Eq. (6.2), the diffracted ray is given by the modified form of σ_{11} of Section 5.6 (or Eq. (5.50)).

$$\tilde{u}_d(\rho_1) \simeq \sqrt{\frac{2}{\pi k \rho_1}}\, e^{ik\rho_1 + i\frac{\pi}{4}} \cdot \frac{\left(\frac{1}{R_1} - \frac{1}{R_2}\right)}{8k} \sum_{s=1}^{\infty} \frac{\sqrt{\pi}\, \exp\left\{i\left(kR_1 + \left(\frac{kR_1}{2}\right)^{1/3} t_s\right)(\phi_1 - \pi)\right\}}{\left(\frac{kR_1}{2}\right)^{1/3} w_1'(t_s)} \tag{6.4}$$

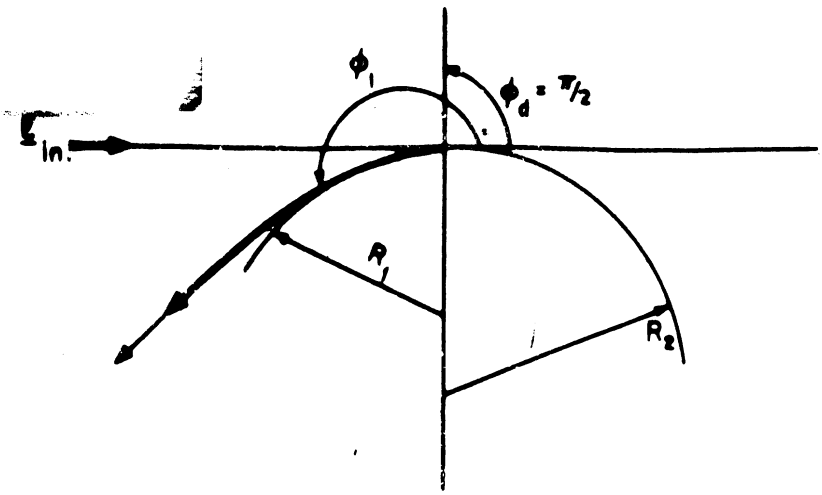

FIG. 6.3: THE RAY DIFFRACTED BY THE EDGE; $\phi_1 > \pi$ AND $\phi_d = \frac{\pi}{2}$

When the point of discontinuity lies at the shadow boundary and the observation point is near the shadow boundary or in the shadow region, the two creeping waves launched by the shadow boundary and by the discontinuity in curvature become indistinguishable. The study of Section 5.5 and Appendix B shows that in such a case the effect of the discontinuity in curvature disappears in the first order term of the asymptotic series for high frequencies.

When the point of discontinuity in curvature lies in the shadow region, the incident creeping wave from the shadow boundary can be locally treated as a plane wave incident along the tangential direction. The amplitude and phase of this plane wave are taken to be the same as those of the incident creeping wave near the edge. Therefore, the edge-effects can be obtained by Eqs. (6.3) and (6.4), provided that the amplitude and phase terms of the incident creeping wave are multiplied to the right-hand side of both equations.

Let us discuss the validity of the amplitudes of diffracted rays given above

for an arbitrary difference of the two curvatures at the discontinuity. As discussed in Chapter 4 and 5, the amplitudes of rays diffracted by the discontinuity are determined by the amplitude of the incident wave and by the behavior of the local mapping function near the discontinuity. But since the precise local mapping function for the arbitrary edge is not easily obtainable, we have assumed the scattering body to be almost circular (see Section 4.2). This fact, in turn, compelled us to assume that the difference between a and $\frac{a}{1-\epsilon^2}$ be small for the particular model of the scattering body considered in Chapter 5. So the results of Chapter 6 for the amplitudes of rays diffracted by the discontinuity in curvature can be improved when the more accurate local mapping function, which is valid for arbitrary difference of two curvatures, becomes available. Still we may conjecture that the local behavior of the approximate mapping function obtained in Section 4.2 gives a reasonably accurate local mapping function for an arbitrary difference of the two curvatures. So the results of Eqs. (6.1), (6.2) and (6.3) may be valid for this case.

We can conclude from the present analysis that the effect of the discontinuity in curvature for the far zone scattering field is of the order of $k^{-1}(k\rho_1)^{-1/2}$ times the amplitude of the incident wave at the discontinuity in curvature. In contrast, it is well known that the effect of a kink is of order $(k\rho_1)^{-1/2}$. In general, the effect of the discontinuity in the n-th derivative of the tangent is of order $k^{-n}(k\rho_1)^{-1/2}$, because the order of singularity of the local mapping function near the edge with a discontinuity in the n-th derivative of the tangent is lowered by the factor n (see Section 4.2).

The extension of the present method to the case of a wedge type singularity is not easy. The difficulty is due to the fact that in this case $\left|\frac{dw}{dz}\right|$ near the singular point is either infinite or zero, no matter how close the transformed contour is to the original contour. Therefore, the first term of the iterated series may not be sufficient (see Chapter 2). Rice[17] showed numerically that the iterated series converges after the second iteration for the low frequency scattering problem by a kink. Apparently there is yet no analytical proof of convergence of the iterated series.

Extensions to the Neumann boundary condition are possible, but one should be even more careful, because now the normal derivative of the scattered field is given on the boundary instead of the scattered field itself (see Eq. (2.6)). Therefore, one must transform a normal derivative of the given function through the mapping function F(z) as

$$\left.\frac{\partial \tilde{u}(w)}{\partial n_w}\right|_{\text{on } C_w} = \left.\frac{\partial u\{w = f(z)\}}{\partial n_z}\,\frac{1}{|F'(z)|}\right|_{\text{on } C_z}$$

in place of Eq. (2.11). For the Dirichlet boundary condition, the boundary value is continuously transformed as long as the mapping function itself is continuously defined on the boundary. But for the Neumann boundary condition, the derivative of the mapping function must be continuous in order to transform the boundary value continuously.

APPENDIX A

ASYMPTOTIC FORM OF $\frac{\partial G}{\partial n}$ FOR HIGH FREQUENCY

In this Appendix, the normal derivative of the Green's function for a circular cylinder is asymptotically evaluated for high frequency in terms of the Fock function.

The Green's function which satisfies the Dirichlet boundary condition on a circular cylinder with radius R is given by Eq. (3.12). The series of Eqs. (3.12) is slowly convergent for a large kR. In order to obtain more rapidly converging series for $kR \gg 1$, the Watson transformation is applied to Eq. (3.12).

$$\left.\frac{\partial G(\underline{r}_1, \underline{r})}{\partial n}\right|_{r=R} = \frac{1}{2\pi R} \sum_{n=-\infty}^{\infty} e^{in\psi} \frac{H_n^{(1)}(kr_1)}{H_n^{(1)}(kR)}$$

$$\simeq \sqrt{\frac{2}{\pi kr_1}}\, e^{ikr_1 - i\frac{3\pi}{4}} \frac{1}{4\pi R} \int_{C_1 + C_2} d\nu \frac{e^{i\nu(\psi - \frac{3\pi}{2})}}{H_\nu^{(1)}(kR) \cdot \sin\nu\pi} \qquad \text{(A-1)}$$

where

$$\psi \equiv \theta - \theta_1 .$$

Changing the contour C_2 into C_1 and using the following relationship

$$2i \sin\nu\pi \cdot e^{+i\nu\frac{\pi}{2}} = e^{i\nu\frac{3\pi}{2}} - e^{-i\nu\frac{\pi}{2}}$$

Eq. (A-1) becomes

$$\left.\frac{\partial G}{\partial n}\right|_{r=R} \simeq \sqrt{\frac{2}{\pi kr_1}}\, e^{ikr_1 - i\frac{\pi}{4}} \left[I_1 + I_2\right] \qquad \text{(A-2)}$$

where

$$I_1 = -\frac{1}{\pi R} \int_{C_1} d\nu \, \frac{e^{i\nu\frac{\pi}{2}} \cos\nu(\psi-\pi)}{H_\nu^{(1)}(kR)} \qquad \text{(A-3)}$$

and

$$I_2 = -\frac{i}{2\pi R} \int_{C_1} d\nu \, \frac{e^{i\nu\frac{3\pi}{2}} \cos\nu(\psi-\pi)}{\sin\nu\pi \, H_\nu^{(1)}(kR)} \qquad \text{(A-4)}$$

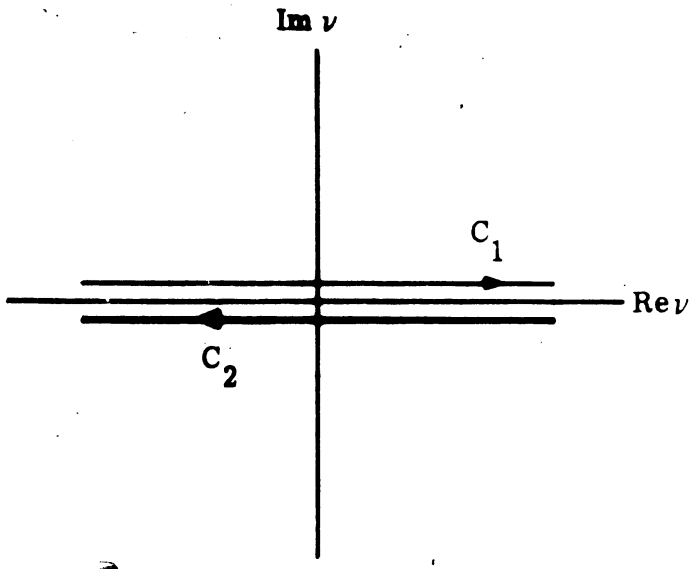

FIG. A-1: THE CONTOURS C_1 AND C_2

For the evaluation of I_1, the contour C_1, can be changed into the contour of Figure A-2 if $\pi/2 \leq \psi \leq 3\frac{\pi}{2}$ (see Gorianov's paper[9]).

Using the asymptotic formula given by Fock[3] in Eq. (A-3)

$$H_\nu^{(1)}(kR) = -i \frac{w_1(t)}{\sqrt{\pi}\, M} , \qquad (A-5)$$

where

$$\nu = kR + Mt$$

$$M = \left(\frac{kR}{2}\right)^{1/3}$$

and

$w_1(t)$ is an Airy function,

we obtain

$$I_1 = \frac{ki}{4M} \left[e^{ikR(\psi - \frac{\pi}{2})} \tilde{f}\left\{\zeta = M(\psi - \frac{\pi}{2})\right\} + e^{ikR(\frac{3\pi}{2} - \psi)} \tilde{f}\left\{\zeta = M(\frac{3\pi}{2} - \psi)\right\} \right]$$

$$\text{for } \pi/2 \leq \psi \leq \frac{3}{2}\pi . \qquad (A-6)$$

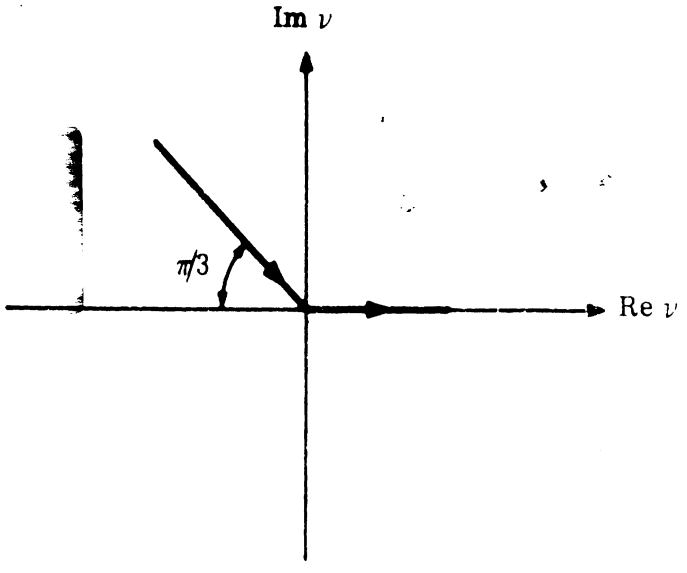

FIG. A-2: THE ⌐ CONTOUR

$\tilde{f}(\zeta)$ is called the Fock function and is given by the following equation

$$\tilde{f}(\zeta) = \frac{1}{\sqrt{\pi}} \int_{\Gamma} \frac{e^{i\zeta t}}{w_1(t)}\, dt \qquad (A\text{-}7)$$

The property of the Fock function is given by Eqs. (4.17), (4.18), and (4.19).

When $\pi/2 > \psi \geq 0$, I_1 can be changed into another form as discussed in Section 4.1

$$kR\cos\psi \simeq -ikR(\psi - \frac{\pi}{2}) + \frac{M^3}{3}(\psi - \frac{\pi}{2})^3 \quad \text{near } \psi \simeq \frac{\pi}{2}\,. \qquad (A\text{-}8)$$

Using Eq. (4.18) and (A-7), I_1 can be written as

$$I_1 \cong -\frac{ik}{2}\cos\psi\, e^{-ikR\cos\psi} + \frac{ki}{4M}\, e^{ikR(\frac{5}{2}\pi - \psi)}\, \tilde{f}\left\{\zeta = M(\frac{5}{2}\pi - 4)\right\}$$

$$\text{for } 0 \leq \psi < \frac{\pi}{2}. \qquad (A\text{-}9)$$

For the evaluation of I_2, the contour C_1 can be changed into Γ for all ψ. Using the same method as I_1 and the following relationship

$$\frac{1}{\sin\nu\pi} = -2i \sum_{n=1}^{\infty} e^{i\nu(2n-1)\pi} \quad \text{for } \mathrm{Im}\,\nu > 0$$

we obtain

$$I_2 = \frac{ki}{4M} \sum_{n=1}^{\infty} \left[e^{ikR(\psi - \frac{\pi}{2} + 2n\pi)}\, \tilde{f}\left\{\zeta = M(\psi - \frac{\pi}{2} + 2n\pi)\right\} \right.$$

$$\left. + e^{ikR(\frac{3}{2}\pi - \psi + 2n\pi)} \cdot \tilde{f}\left\{\zeta = M(\frac{3}{2}\pi - \psi + 2n\pi)\right\} \right]\,. \qquad (A\text{-}10)$$

APPENDIX B

THE SADDLE POINT CONTRIBUTION

In this Appendix, one of the branch cut integrals due to the saddle points in Eq. (4.12) is asymptotically evaluated for both Case I ($\pi \geq \phi_1 > 0$) and Case II ($\phi_1 = 0$). This integral is identified as the contribution of specularly reflected fields for Case I and as that of fields diffracted by the shadow boundary for Case II.

Equation (4.12) is given as

$$\tilde{\sigma} = -i\frac{M^2}{2}\int_{\tilde{v}(\theta=\pi)}^{-i\infty} e^{-\tilde{v}}\frac{d\theta}{d\tilde{v}}\left[1+g(-\theta+\pi+\phi_1)\right]\cdot\tilde{f}\left\{\zeta=M(\frac{\pi}{2}-\theta)\right\}. \quad \text{(B-1)}$$

Equation (B-1) is obtained by inserting $\theta_1 = \phi_1$ for the inverse transformation of the far field (see Eq. (4.14)). For our particular model of the scattering body in Chapter 5 (see Fig. 5-1)), $g(-\theta+\pi+\phi_1)$ is given by Eq. (5.1).

By Eq. (5.9) one of the saddle points is found at

$$\begin{aligned} \theta = \theta'_{so} &= \frac{\phi_1}{2} + \frac{\pi}{2} \quad \text{for Case I} \\ \theta = \theta_{so} &= \phi_1 + \frac{\pi}{2} \quad \text{for Case II} \end{aligned} \quad \text{(B-2)}$$

The saddle contribution of Eq. (B-1) for Case I and Case II can be written as a branch cut integral near this saddle point as discussed in Section 4.1 (see Fig. 5-2).

$$\tilde{\sigma}_s = -i\frac{M^2}{2}\int_{C'_{so}\text{ or }C_{so}} e^{-\tilde{v}}\frac{d\theta}{d\tilde{v}}\left[1+g(-\theta+\pi+\phi_1)\right]\cdot\tilde{f}\left\{\zeta=M(\frac{\pi}{2}-\theta)\right\} \quad \text{(B-3)}$$

Case I: $\pi \geq \phi_1 > 0$

Near the saddle point $\theta = \frac{\phi_1}{2} + \frac{\pi}{2}$, ζ becomes a negative quantity. Using the asymptotic form of the Fock function for the negative argument (see Section 4.1) $\tilde{v}$ becomes

$$\tilde{v} = ikR\left[\cos(\phi_1 - \theta) - \cos\theta\right]$$
$$\simeq i2kR \sin\frac{\phi_1}{2} + \tau^2 ikR \sin\frac{\phi_1}{2} \qquad \text{(B-4)}$$

where

$$\tau = \theta - \theta'_{so} .$$

Define

$$v = -ikR \sin\frac{\phi_1}{2}\, \tau^2$$

$$\tau_+ = \frac{e^{i\frac{\pi}{4}} v^{1/2}}{\sqrt{kR \sin\frac{\phi_1}{2}}} \qquad \text{for Im } v > 0 \qquad \text{(B-5)}$$

$$\tau_- = \frac{e^{i\frac{5\pi}{4}} v^{1/2}}{\sqrt{kR \sin\frac{\phi_1}{2}}} \qquad \text{for Im } v < 0 .$$

If ϕ_1 is not near $2(\phi_d - \frac{\pi}{2})$ such that the specular reflection point is far from the point of discontinuity in curvature (see section 5.2), $g(-\theta + \frac{\pi}{2} + \phi_1)$ is analytic near this saddle point. Considering only the dominant term for $kR \gg 1$, $\tilde{\sigma}_s$ becomes

$$\tilde{\sigma}_s \sim \frac{kR}{2} \cos\left(\frac{\pi}{2} + \frac{\phi_1}{2}\right) e^{-i2kR \sin\frac{\phi_1}{2}}$$

$$\cdot \int_0^\infty dv\, e^{-v} \left\{ \left[1 + g\left(\frac{\pi}{2} + \frac{\phi_1}{2} - \tau_-\right)\right] \frac{d\tau_-}{dv} - \left[1 + g\left(\frac{\pi}{2} + \frac{\phi_1}{2} - \tau_+\right)\right] \frac{d\tau_+}{dv} \right\}$$

$$\simeq \sqrt{\frac{\pi kR \sin\frac{\phi_1}{2}}{2}}\, e^{i\frac{\pi}{4}} \cdot \left[1 + g\left(\frac{\pi}{2} + \frac{\phi_1}{2}\right)\right] . \qquad \text{(B-6)}$$

When $\phi_1 = 2(\phi_d - \frac{\pi}{2})$, the branch point of $g(-\theta + \frac{\pi}{2} + \phi_1)$ coincides with the saddle point $\frac{\phi_1}{2} + \frac{\pi}{2}$. However, since the first derivative of $g(-\theta + \frac{\pi}{2} + \phi_1)$ with respect to θ is a continuous function near this branch point (see Section 4.2), we obtain the same result as Eq. (B-6) even in the case of $\phi_1 \simeq 2(\phi_d - \frac{\pi}{2})$.

By Eq. (4.7) and (B-6) the contribution of the saddle point at $\theta = \frac{\phi_1}{2} + \frac{\pi}{2}$ becomes

$$\tilde{u}_{s.r.}(\rho_1) \simeq -\sqrt{\frac{\pi kR \sin\frac{\phi_1}{2}}{2}} \left[1 + g\left(\frac{\pi}{2} + \frac{\phi_1}{2}\right)\right] \sqrt{\frac{2}{\pi k\rho_1}}\, e^{ik\rho_1} \qquad \text{(B-7)}$$

Eq. (B-7) represents the specularly reflected field for both cases when the specular reflection point and the point of the discontinuity in curvature are far apart, and when they coincide.

Case II: $\phi_1 \simeq 0$

In this case the saddle point lies at $\theta_{so} = \frac{\pi}{2} + \phi_1$ instead of $\theta_{so'} = \frac{\pi}{2} + \frac{\phi_1}{2}$. Near $\theta = \frac{\pi}{2} + \phi_1$, the argument of the Fock function becomes zero as ϕ_1 approaches

zero. So near $\theta = \frac{\pi}{2} + \phi_1$

$$\tilde{v} = ikR\left[\cos(\phi_1 - \theta) + \theta - \frac{\pi}{2}\right]$$
$$\simeq ikR\,\phi_1 + iM^3\frac{\tau^3}{3} \qquad \text{(B-8)}$$

where

$$\tau \equiv \theta - \frac{\pi}{2} - \phi_1$$

Let

$$v = iM^3\frac{\tau^3}{3}$$

$$\tau_+ = \frac{\tilde{\beta}\, v^{1/3}}{M} \qquad \text{for Im } v > 0$$

$$\tau_- = \frac{\beta\, v^{1/3}}{M} \qquad \text{for Im } v < 0 \qquad \text{(B-9)}$$

where

$$\begin{cases} \tilde{\beta} \equiv (3)^{1/3}\, e^{-i\frac{\pi}{6}} \\ \beta \equiv (3)^{1/3}\, e^{-i\frac{5\pi}{6}} \end{cases}$$

$g(-\theta + \pi + \phi_1)$ is analytic near $\theta = \frac{\pi}{2} + \phi_1$ unless $\phi_d = \frac{\pi}{2}$. When $\phi_d = \frac{\pi}{2}$ the point of discontinuity in curvature lies at the shadow boundary, and two branch cuts at $\theta = \frac{\pi}{2} + \phi_1$ and at $\theta = \theta_{do} = \phi_1 - \phi_d + \pi$ coincide (see Case IV-B of Section 5.5). With the same argument as Case I (i.e. the derivative of the $g(-\theta + \pi + \phi_1)$ near $\theta = \theta_{do}$ is continuous), for Case II, $\tilde{\sigma}_s$ becomes

$$\tilde{\sigma}_s \simeq -i\frac{M^2}{2}\left[1 + g\left(\frac{\pi}{2}\right)\right] \cdot I_s \qquad \text{(B-10)}$$

for both cases when the point of the discontinuity and the shadow boundary are far apart and when they coincide. Here I_s is given as

$$I_s = \frac{1}{\sqrt{\pi}} \int_{\Gamma} dt\, e^{-i(kR+Mt)\phi_1} \left[\int_0^{\infty} dv\, e^{-v} \left\{ \frac{d\tau_-}{dv} \cdot \exp(-it\beta v^{1/3}) - \frac{d\tau_+}{dv} \cdot \exp(-it\tilde{\beta} v^{1/3}) \right\} \right]$$

$$= \frac{1}{\sqrt{\pi}} \int_{\Gamma} dt\, e^{-i(kR+Mt)\phi_1} \left[-\frac{e^{i\frac{\pi}{6}}}{M} \left\{ \int_0^{\infty} e^{-\frac{x^3}{3} + te^{i\frac{2}{3}\pi}x}\, dx \right.\right.$$

$$\left.\left. + \int_{\infty \exp(i\frac{2}{3\pi})}^{0} e^{\frac{-x^3}{3} + tx \exp(i\frac{2}{3}\pi)}\, dx \right\} \right]$$

$$= \frac{1}{\sqrt{\pi}} \int_{\Gamma} dt\, \frac{e^{-i(kR+Mt)\phi_1}}{w_1(t)} \left[-\frac{e^{i\frac{\pi}{6}}}{M} \sqrt{\pi}\, w_2(t\, e^{i\frac{2}{3}\pi}) \right]$$

$$= -\frac{2}{M\sqrt{\pi}} \int_{\Gamma} dt\, \frac{Ai(t)}{w_1(t)}\, e^{-i(kR+Mt)\phi_1} \qquad \text{(B-11)}$$

Here $Ai(t) = \frac{\sqrt{\pi}}{2i} \left\{ w_1(t) - w_2(t) \right\}$ is an Airy function. By Eq. (4.7) and (B-11), the saddle point contribution at $\theta = \frac{\pi}{2} + \phi_1$ for Case II becomes

$$\tilde{u}_{c.w.}(\rho_1) \simeq \frac{M}{\sqrt{\pi}} \left[1 + g(\tfrac{\pi}{2}) \right] \left[\int_{\Gamma} dt\, \frac{Ai(t)}{w_1(t)}\, e^{-i(kR+Mt)\phi_1} \right] \sqrt{\frac{2}{\pi k \rho_1}}\, e^{ik\rho_1 + i\frac{\pi}{4}} \qquad \text{(B-12)}$$

When ϕ_1 becomes negative (B-12) can be expanded as a residue series

$$\tilde{u}_{c.w.}(\rho_1) \sim 2M \left[1 + g(\tfrac{\pi}{2}) \right] \left[\sum_{s=1}^{\infty} \frac{Ai(t_s)}{w_1'(t_s)}\, e^{-i(kR+Mt_s)\phi_1} \right] \sqrt{\frac{2}{k\rho_1}}\, e^{ik\rho_1 + i\frac{3\pi}{4}}$$

$$\text{for } \phi_1 < 0. \qquad \text{(B-13)}$$

Equation (B-13) represents the contribution of creeping waves which are diffracted near the upper shadow boundary.

Equation (B-12) and (B-13) hold both when the shadow boundary and the point of discontinuity in curvature are far apart and when they coincide.

NOTATION

C_d, C_d^*, $\overline{C}_d$ and $\overline{C}_d^*$	:	Contours around the branch cuts due to the singularity of the mapping function.
C_s and C_s^*	:	Contours around the branch cuts due to the saddle points.
δ	:	The boundary perturbation factor.
$\tilde{f}(\zeta)$	:	Fock function.
$F(z) = z + \delta f(z)$	:	Mapping function.
$g(\theta) = ik\delta \mathrm{Re} f(z=Re^{i\theta})$	:	The real part of $F(z)-z$ on the boundary multiplied by ik.
ϕ_d	:	The angle between the propagation direction of the incident wave and the normal direction of the boundary at the edge.
θ_d and $\overline{\theta}_d$	:	The branch points of the mapping function due to the edge at $\phi=\phi_d$ (Fig. 5.1).
θ_d^* and $\overline{\theta}_d^*$	:	The branch points of the mapping function due to the edge at $\phi=\phi_d-\pi$ (Fig. 5.1).
θ_s and θ_s^*	:	The saddle points.
$\tilde{u}(w = F(z)) = u(z)$	:	The z-component of the scattered field.
$\tilde{u}_{s.r.}$	:	The specularly reflected field.
$\tilde{u}_{c.w.}$	:	The creeping waves from the shadow boundary.
$\tilde{u}_d$	:	The fields diffracted by the edge.
$\tilde{u}_p$	:	The perturbed field.
$z = x + iy = re^{i\theta}$	:	The coordinate system of the transformed domain.
$w = \xi + i\eta = \rho e^{i\phi}$	:	The coordinate system of the original domain.
$\rho_1 = \rho_1 e^{i\phi_1}$	:	The observation point.

BIBLIOGRAPHY

(1) J. VanBladel, "Low-Frequency Scattering by Cylindrical Bodies," Appl. Sci. Res., Vol. B-10, pp. 195-202; 1963.

(2) H. M. Macdonald, "The Effect Produced by an Obstacle on a Train of Electric Waves," Philos. Trans. Roy. Soc. London, Vol. A-212, pp. 299 - 337; 1913.

(3) V. Fock, "Diffraction of Radio Waves around the Earth's Surface," J. of Phys., Vol. 9, pp. 255 - 266; 1945.

(4) V. Fock, "The Distribution of Currents Induced by a Plane Wave on the Surface of a Conductor," J. of Phys., Vol. 10, pp. 130-136; 1946.

(5) W. Franz and K. Depperrmann, "Theory of Diffraction by a Cylinder as Affected by the Surface Wave," Ann. Physik., Vol. 10, pp. 361 - 373; 1952.

(6) W. Franz, "On the Green's Functions of the Cylinder and the Sphere," Z. für Naturforschung, Vol. 9A, pp. 705 - 716; 1954.

(7) J. B. Keller, "Diffraction by a Convex Cylinder," IRE Trans. On Antennas and Propagation, Vol. Ap-4, pp. 312 - 321; 1956

(8) F. Ursell, "On the Short-Wave Asymptotic Theory of the Wave Equation $(\nabla^2 + k^2)\phi=0$," Proc. Cambridge Philos. Soc., Vol. 53, pp. 115 - 133; 1957.

(9) A. S. Goriainov, "An Asymptotic Solution of the Problem of Diffraction of a Plane Electromagnetic Wave by a Conducting Cylinder," Radiotekhnika i elektronika, Vol. 3, pp. 23 - 39; 1958.

(10) R. F. Goodrich, "Fock Theory - An Appraisal and Exposition, "IRE Trans. On Antennas and Propagation, Vol. Ap-7, pp. 528 - 536; 1959.

(11) L. A. Weinstein and A. A. Fedorov, "Scattering of Plane and Cylindrical Waves on an Elliptical Cylinder and Conception of Diffraction of Rays," Radiotekhnika i elektronika, Vol. 6, pp. 31 - 46; 1961.

(12) L. B. Felsen, "Quasi-Optic Diffraction," Quasi-Optics, Polytech. Press of Polytech. Inst. of Brooklyn, pp. 1 - 40; 1964.

(13) F. Oberhettinger, "Diffraction of Waves by a Wedge," Comm. Pure and Appl. Math., Vol. 7, pp. 551 - 563; 1954.

(14) J. B. Keller, "Diffraction by Polygonal Cylinders" Electromagnetic Waves edited by R. Langer, The Univ. of Wisconsin Press, pp. 129 - 137; 1962.

(15) V. H. Weston, "The Effect of a Discontinuity in Curvature in High-Frequency Scattering," IRE Trans. On Antennas and Propagation, Vol. Ap-10, pp. 775 - 780; 1962.

(16) V. H. Weston, "Effect of a Discontinuity of Curvature in High-Frequency Scattering, Part II," IEEE Trans. On Antennas and Propagation, Vol. Ap-13, 1965.

(17) S. O. Rice, "Reflection from Corners in Rectangular Wave Guides-Conformal Transformation," Bell Syst. Tech. J., Vol. 28, pp. 104-135; 1949.

(18) S. O. Rice, "A Set of Second-Order Differential Equations Associated with Reflection in Rectangular Wave Guides - Application to Guide Connected to Horn," Bell Syst. Tech. J., Vol. 28, pp. 136-156; 1949.

(19) L. A. Weinstein, "The Method of Approximate Separation of Variables and its Application to the Boundary Problems of Electrodynamics and Acoustics," Z. Technicheskoi Fiziki, Vol. 27, pp. 2109 - 2128; 1957.

(20) R. Mittra, "Solution of Boundary Value Problems in Nonuniform and Inhomogeneously-Filled Waveguides," University of Toronto Antenna Laboratory Research Report No. 9; 1957.

(21) H. H. Meinke, "A Survey on the Use of Conformal Mapping for Solving Wave Field Problems," Electromagnetic Theory and Antennas, edited by E. C. Jordan, Pergamon Press, pp. 1113 - 1124; 1964.

(22) D. S. Jones, "High-Frequency Refraction and Diffraction in General Media," Philos. Trans. Roy. Soc. London, Vol. A-255, pp. 341 - 387; 1963.

(23) P. R. Garabedian, "An Integral Equation Governing Electromagnetic Waves," Quart. Appl. Math., Vol. 12, pp. 428 - 433; 1955.

(24) S. E. Warschawski, "On the Higher Derivatives at the Boundary in Conformal Mapping," Trans. Am. Math. Soc., Vol. 38, pp. 310 - 340; 1935.

(25) Z. Nehari, Conformal Mapping, McGraw-Hill, pp. 263-265; 1952.